Fast-ion-beam laser-induced-fluorescence measurements of spontaneous-emission branching ratios and oscillator strengths in Sm II

S.J. Rehse, R. Li, T.J. Scholl, A. Sharikova, R. Chatelain, R.A. Holt, and S.D. Rosner

Abstract: We measured the spontaneous-emission branching ratios of 69 levels in Sm II selectively populated via single-frequency laser excitation of a 10 keV ion beam. The levels studied had term energies up to 29 600 cm^{-1}, and decay branches with spontaneous emission in the range 250–850 nm were detected. The experimental accuracy was in the range of 10%. We used these branching ratios along with our previously determined radiative lifetimes to infer transition probabilities and oscillator strengths for 608 transitions in the wavelength range 363–771 nm, which are useful for stellar abundance determinations.

PACS Nos.: 32.70.Cs, 95.30.Ky

Résumé : Nous avons mesuré les rapports de branchement d'émission spontanée de 69 niveaux du Sm II peuplés de façon sélective par excitation laser à fréquence unique d'un faisceau d'ions de 10 keV. Les niveaux excités avaient des terme d'énergies jusqu'à 29 600 cm^{-1} et nous avons détecté des branches de désexcitation avec émission spontanée de 250 à 850 nm. La précision expérimentale était de l'ordre de 10 %. Nous avons utilisé ces rapports de branchement avec des temps de vie radiatifs préalablement obtenus pour déterminer les probabilités de transition et les forces d'oscillateur de 608 transitions dans le domaine de longueur d'onde de 363 à 771 nm qui sont utiles pour fixer les abondances stellaires.

[Traduit par la Rédaction]

1. Introduction

A knowledge of the atomic properties of the lanthanide ions is vital to astrophysical studies of chemically peculiar (CP) stars of the upper main sequence, metal deficient stars of the galactic halo, and the Sun [1, 2]. The lanthanides are present in CP stars in great excess in comparison with solar

Received 3 December 2005. Accepted 15 May 2006. Published on the NRC Research Press Web site at http://cjp.nrc.ca/ on 16 September 2006.

S.J. Rehse, R. Li, T.J. Scholl, A. Sharikova, R. Chatelain, R.A. Holt, and S.D. Rosner.[1] Department of Physics and Astronomy, University of Western Ontario, London, ON N6A 3K7, Canada.

[1] Corresponding author (e-mail: rosner@uwo.ca).

 doi: 10.1139/P06-063

abundances; for example, in the rapidly rotating star HD101065 (Przybylski's star), Sm II has an excess of 3.6 dex (a factor of 4×10^3) compared with its solar abundance [3]. In CP stars with measurable magnetic-field effects, the spectral lines of the lanthanide elements are among the most enhanced [2]. The galactic halo stars, which are among the oldest stars in our galaxy, have the potential to reveal the secrets of nucleosynthesis in novae and supernovae. The lanthanides, in particular, form a contiguous sequence of atomic numbers which allow astrophysicists to study the odd–even effect resulting from the nuclear pairing interaction, and they present numerous examples of isotopes that may be formed by the r-process, the s-process, the p-process, or a combination. In the case of Sm, of the seven stable isotopes, ^{148}Sm and ^{150}Sm are produced in the stars by the s-process; ^{144}Sm by the p-process; ^{154}Sm by the r-process; and ^{147}Sm, ^{149}Sm, and ^{152}Sm by both the r- and s-processes. The study of lanthanides in the solar spectrum is experiencing a resurgence of interest with the availability of satellite spectra in the UV and laboratory data from new techniques. The potential contribution of two free electrons to the solar opacity by the lanthanides, the realization that diffusion, which has had a significant fractionating effect on helium [4], may well have affected the heavier elements in the Sun, and increasing caution with regard to the accuracy of meteoritic abundances have all contributed to this renewed interest. Beyond astrophysics, the atomic properties of the lanthanides are needed in the design of commercial high-intensity discharge lamps [5] and in the use of spectra to probe the crystalline structure of divalent and trivalent crystal salts [2].

For a transition of known wavelength, the most important atomic property for astrophysics is its oscillator strength f. In the case of Sm II, only a very small number of experiments have provided published data of modest accuracy. In the 1930s Meggers began a program of intensity measurements at the National Bureau of Standards that led to a number of monographs listing intensities [6, 7] and oscillator strengths [8]. In the later version of these experiments, 0.1 atomic per cent of the element under study was incorporated in the Cu electrodes of a DC arc discharge, and the spectrum was measured with a rotating stepped sector to decrease the intensity of a line until it reached the limit of photographic detectability, from which a linear measure of the line intensity could be obtained. Assumptions about local thermodynamic equilibrium, rate of entry and exit of atoms from the discharge, and negligible self-absorption were then used by Corliss and Bozman [8] to determine absolute transition probabilities. They estimated the overall uncertainty in log gf as varying from 0.24 to 0.29 (corresponding to almost a factor of 2 in gf) as the upper-level term energy varied from 1.5×10^4 to 5.0×10^4 cm^{-1}. (g is the multiplicity $2J + 1$ of the lower state).

A more accurate approach to determining oscillator strengths is to combine data on the branching ratios (BRs) for all transitions from a given level with a value for the spontaneous emission lifetime of that level. Saffman and Whaling [9] measured BRs in a hollow-cathode discharge and incorporated the beam-foil lifetime measurements of Andersen et al. [10] to obtain oscillator strengths for transitions from 9 levels of Sm II. Kurucz [11] compiled experimental oscillator strengths in a form that is available online [12], using the data of Saffman and Whaling, BRs from the intensity measurements of Meggers et al., together with experimental lifetime data.

Kastberg et al. [13] used optical nutation with a fast Doppler switching technique in collinear fast-ion-beam laser spectroscopy to measure the absolute transition probabilities for three lines of Sm II; the combined statistical and systematic uncertainties were on the order of 10%.

Quite recently, Xu et al. [14] performed relativistic Hartree–Fock (HFR) calculations of BRs for 47 levels and combined them with their own time-resolved laser-induced-fluorescence lifetime measurements to calculate oscillator strengths for 162 transitions; these are available online from the DREAM database [15]. The estimated uncertainties in the oscillator strength determinations were assigned one of three values: 10%, 30%, or 50%.

Previously to the work of Xu et al. our own group measured the spontaneous-emission lifetimes of 82 levels in Sm II with a fast-ion-beam laser-induced-fluorescence technique [16]. A comparison of the two sets of results showed agreement within experimental error (a few percent in both cases), although

Fig. 1. Apparatus for branching-ratio measurements. A 100 nA Sm II beam is overlapped with a collinear antiparallel single-frequency cw laser beam tuned to excite a Doppler-shifted energy level in a post-acceleration region whose potential is modulated at 5 kHz. Fluorescence from all the decay branches is collected with arrays of optical fibers, spectrally analyzed in a Czerny–Turner monochromator, and detected by a photomultiplier connected to a lock-in amplifier. A second identical monochromator set to the wavelength of one of the decay branches provides a normalization signal. A data acquisition computer controls wavelength scanning of the monochromator and records the laser-induced fluorescence intensity as a function of wavelength, as well as the ion current, laser power, and the output of the normalization channel. A third lock-in amplifier is used to stabilize the dye-laser frequency against wavelength drift.

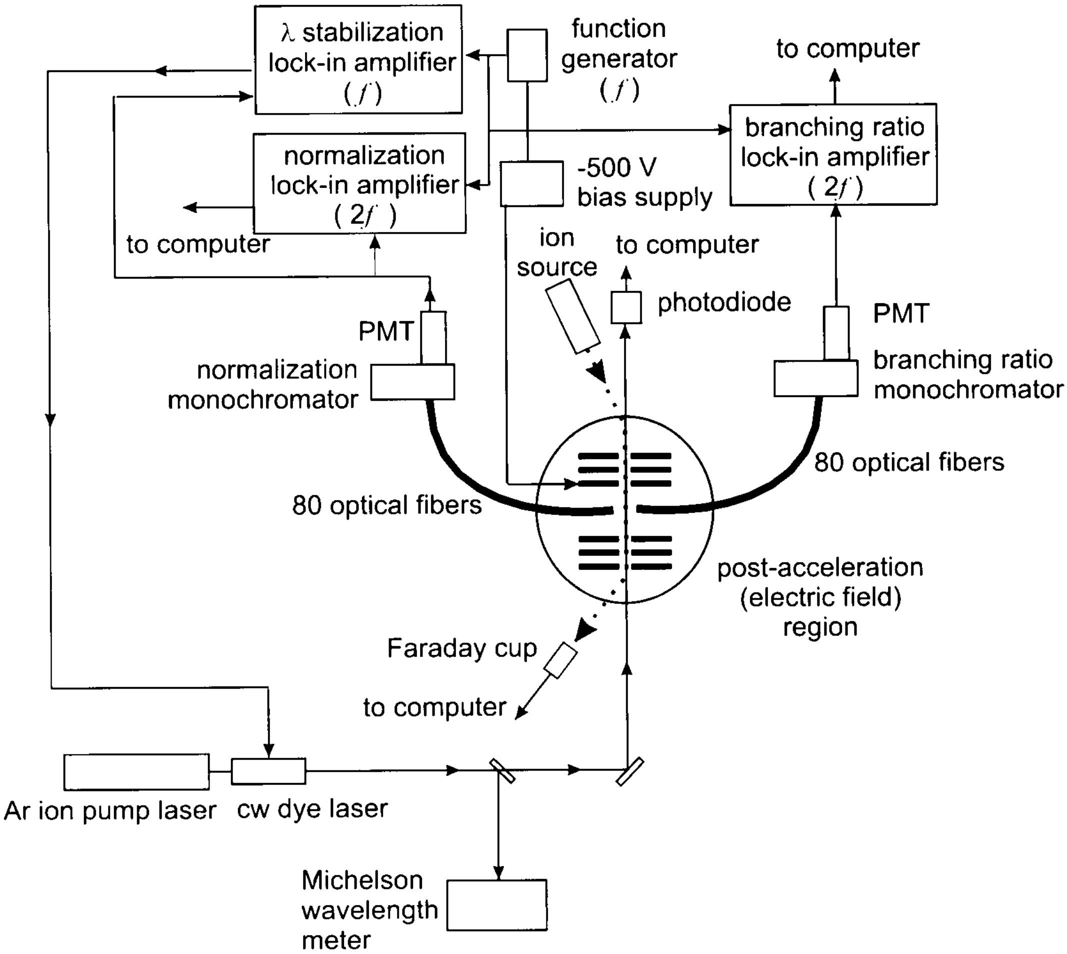

there was a hint of a systematic divergence for lifetimes longer than 60 ns. In the current work, we have carried out a measurement of BRs for all levels whose lifetimes we determined in our previous study, using a new fast-ion-beam technique to be described in more detail in the following section. Using the spectrum of laser-induced fluorescence from a velocity-modulated 10 keV ion beam to measure BRs, we can identify with certainty the transitions that belong to a common upper level, and the uncluttered spectra avoid most problems due to blended lines.

2. Experimental method

Branching ratios for an excited atomic state are typically measured by observing the spectrum of spontaneous emission from that state and measuring the relative intensities of the spectral lines. Previous determinations of branching ratios in lanthanides have utilized a hollow-cathode discharge lamp with the element of interest contained in the cathode cavity [17]. The energy level structure in the lanthanides is quite rich and the spontaneous emission from many levels in several ionization states is present in such discharges, creating potential systematic errors due to spectral blending. To properly identify the branches from specific levels of interest, comparison with previous measurements or a priori calculations are necessary. Even still, given the sparse knowledge of the levels of Sm II, the possibility exists for the misidentification of emission lines by either omitting a branch from its correct level or attributing to a level an emission that actually emanates from a different excited state.

The "beam-laser" method is a much more reliable spectroscopic technique that involves selective excitation of a single state in a single-species ion beam followed by direct observation of the subsequent laser-induced fluorescence [18]. All decay branches originating from this selectively populated state with a transition wavelength within the spectral viewing range are observed and can be assigned with absolute certainty to that excited state. Also, the signal-to-noise ratio (SNR) provided by laser excitation is excellent for typical conditions of integration times of ~1 s or greater and ion currents of ~50 nA or greater.

A schematic of our experimental apparatus is shown in Fig. 1. Sm^+ ions were produced in a modified Danfysik 911A source without an arc discharge; ionization occurred on the surface of a hot tungsten filament. Under such conditions, we observed stable beams of ions produced in metastable levels up to ~7100 cm^{-1}. Ion-beam currents of ~100 nA were typical and the actual current as detected by a secondary-electron-suppressed Faraday cup was monitored by a data acquisition computer. After acceleration to 10 keV, the ions were focused, mass-filtered by a Wien velocity filter, and then electrostatically deflected to overlap a counter-propagating laser beam. Collinear geometry has three advantages, arising from the Doppler effect. The spatial extent of the excitation region can be limited by utilizing the Doppler shift produced in a post-acceleration process. Modulation of the post-acceleration field and phase-sensitive fluorescence detection yields background-suppressed signals. Also, collinear geometry creates a kinematic compression of the Doppler width, which increases signal size and makes the excitation process more selective [19]. Our absorption Doppler width arose primarily from the spread in the kinetic energy of the ions, resulting in linewidths of ~200 MHz for our beam velocities and laser frequencies, compared to ~2 GHz in the case of the two beams crossing at 90°.

The single-frequency laser beam was produced by an argon-ion-pumped Coherent 699-21 dye laser running with Stilbene 3 dye. Stilbene 3 has a nominal tuning curve from 415–465 nm, so only Sm II levels that could be excited via transitions within this wavelength range were studied. The laser wavelength was determined to ~1 part in 10^7 by a traveling Michelson interferometer with a polarization-stabilized reference helium–neon laser [20, 21]. In the area of laser excitation and fluorescence, the laser beam was softly focused to a 0.5 mm radius waist by a 2 m focal-length lens. Prior to entering the ion-beam vacuum chamber, the laser beam passed through multiple irises to eliminate laser light scattered from upstream optical elements.

Ion resonance with the antiparallel propagating laser beam was confined to a small region with a high degree of optical access by a modification of the "Doppler-switching" technique [22]. The ions were accelerated (and symmetrically decelerated) in regions of an electric field shaped by eight parallel conducting aperture plates separated by insulating ceramic beads (hereafter referred to as the "post-acceleration region"). A photograph of the ~9 cm long post-acceleration region and the optical fibers used to collect laser-induced fluorescence is shown in Fig. 2. Modeling of the potential by numerical solution of Laplace's equation allowed us to create a highly uniform potential in the ~3 cm central region. As the ions entered this region, they were accelerated by the field and brought into resonance

Fig. 2. The post-acceleration region and optical fibers. Careful shaping of the electric field creates a −500 V flat potential "step" between the parallel plates. In this ~9 cm long region, the laser beam is Doppler-shifted into resonance with the Sm^+ ions. To allow lock-in detection, an added sinusoidal potential of ~15 Vpp at 5 kHz modulates the Doppler-shifted laser frequency seen by the ions. Two bundles of 80 optical fibers arrayed around the axis of the ion beam/laser beam collect the laser-induced fluorescence and guide it out of the vacuum system.

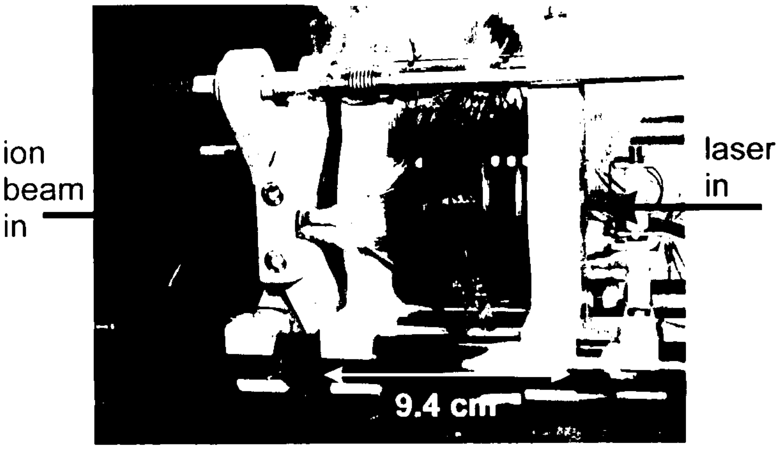

with the Doppler-shifted laser beam. Because the absorption Doppler width corresponded to an energy spread of ~20 V, a potential of this size applied to the central region would have been sufficient to confine the laser-induced fluorescence (LIF) to the vicinity of the optical fiber collectors. In practice we found that the LIF signals increased as this potential was increased because a larger fraction of the Doppler distribution was pumped in view of the fibers, and so a potential of −500 V was used.

Scattered laser light was minimized by careful alignment of the laser beam through a series of apertures on either side of the post-acceleration region. To further suppress the constant background provided by residual scattered laser light and ion collisions with residual gas, the post-acceleration potential was modulated at 5 kHz, providing an AC component to the LIF that was detected with lock-in amplifiers. After passing through the post-acceleration region, the laser beam exited the ion-beam vacuum chamber to a photodiode, where the laser power was measured and recorded by the data acquisition computer. The vacuum system was pumped with three diffusion pumps and the pressure in the source chamber during operation was around 7×10^{-7} Torr (9.3×10^{-5} Pa), while the laser/ion interaction region pressure was around 7×10^{-6} Torr (9.3×10^{-4} Pa).

The LIF was viewed by two arrays of polyimide-coated quartz/quartz optical fibers (Optran-UV from SOMTA, Ltd) with >99%/m transmission from 390 to 850 nm. The outer diameter of the polyimide jacket was 685 μm. The LIF from one array was used for branching-ratio data while the other provided a "normalization" signal that was used to correct the branching-ratio signal for variations in the excitation rate due to drifts in the properties of the laser and ion beams. Each array was composed of 80 fibers (160 fibers total), whose in-vacuum ends were disposed in four rings surrounding the LIF region. The four rings of one array were interleaved with the four rings of the other. The outer ends of the 80 fibers of each array were bundled into a rectangle of four columns by 20 rows to match the entrance slits of the monochromators used to spectrally analyze the fluorescence. The fiber bundle dimensions were 3.2 mm wide by 14.2 mm tall. Each bundle passed from the vacuum system via a purpose-built vacuum feedthrough. The geometric light-collection efficiency for a coplanar ring of 20 fibers was 1.1% and the spacing of the rings was such that a passing ion illuminated ~1 ring of each array at any instant.

Fig. 3. Geometry of the 160 fluorescence-collecting fibers. The angle θ is measured with respect to the vertical linear polarization axis of the laser light ($\hat{z}$). The laser is propagating out of the page along the axis of the rings holding the fibers ($\hat{x}$). (a) The "magic" angle geometry. (b) The $\sin\theta$ geometry.

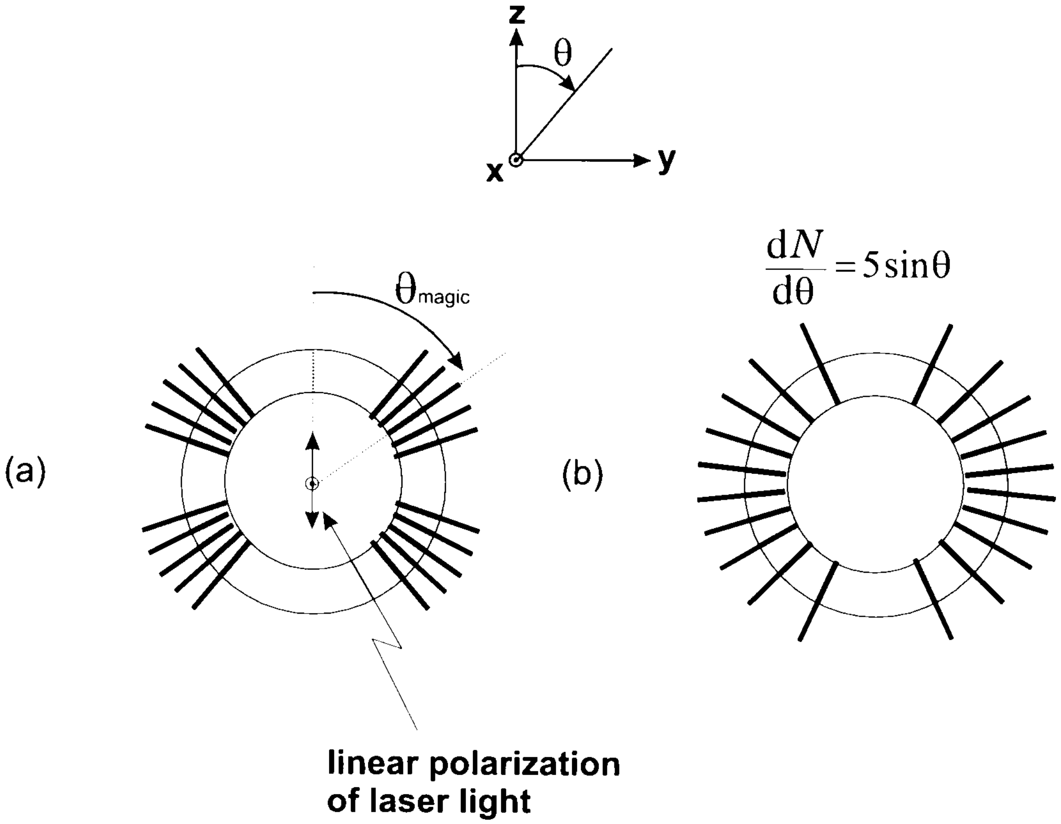

In the centre of the post-acceleration region, each individual fiber was oriented such that its optical axis was perpendicular to the ion/laser axis. The azimuthal positions of the fibers in each array were chosen to eliminate a specific systematic error in the evaluation of the branching ratios that could arise from anisotropic excitation by the linearly polarized laser beam. With the direction of the electric field of the vertically polarized laser defined as $\theta = 0$, the fibers of one array were placed at or near the "magic" angle, $\theta_{\mathrm{magic}} = \cos^{-1}\left(1 \big/ \sqrt{3}\right) \approx 54.7°$, where the angular distribution of fluorescence from $\Delta M = \pm 1$ transitions has the same intensity as that for $\Delta M = 0$ transitions. The fibers of the other array were distributed around a circle in a vertical plane with a density $\mathrm{d}N/\mathrm{d}\theta$ weighted as $\sin\theta$. This spacing ensured that the ratio of detected fluorescence from any two branches was identical to its value in the case of isotropic excitation or detection. These two geometric orientations are illustrated in Fig. 3. Figure 3*a* shows the fibers arranged in the magic angle orientation, while Fig. 3*b* shows the sine weighting. The laser was propagating in the $\hat{x}$ direction (out of the page) at the centre of the rings holding the fibers and was vertically polarized ($\hat{z}$) with respect to the apparatus and fibers. Branching-ratio data were collected with the $\sin\theta$-distributed fibers and the magic-angle bundle collected the normalization signal. A more detailed analysis of the magic-angle and sine-weighted arrays is presented in the Appendix.

Each 80 fiber bundle terminated in a rigid coupling to the input slit of a 0.275 m, $f/3.8$ scanning monochromator (Acton Research Corp.) The 20 mm high slits were normally set at their maximum width of 3 mm. Each monochromator had three gratings on a rotating carousel to provide complete spectral coverage. The gratings had 3600, 2400, and 1200 grooves/mm with a corresponding reciprocal dispersion of 1.0, 1.5, and 3.0 nm/mm, respectively. The first grating provided coverage from 250–500 nm, the second from 250–750 nm, and the third from 250–1500 nm. Since most of the Sm II emission lines have wavelengths shorter than 500 nm, the first two gratings with superior resolution were used for the majority of the measurements, while the infrequent longer wavelength lines were observed with the third grating. In cases where closely spaced emission lines precluded the resolution of individual lines, the entrance and exit slits of the monochromator were narrowed until the individual lines were resolved and the entire spectrum was obtained at that slit width. When measuring branches with wavelengths longer than 600 nm, a long-wavelength-pass filter (50% transmission point at 475 nm) was inserted prior to the PMT to avoid observation of second-order diffraction from the grating.

When it was not possible to record the entire spectrum with sufficient resolution with only one grating, spectra obtained with multiple gratings were pieced together to provide complete spectral coverage. When this was done, care was taken to ensure sufficient spectral overlap of the spectra. Each grating scan contained at least two branches, one of which was recorded by another grating; in some cases the number of branches appearing in both spectra was greater than one. The method for combining the data from two overlapping spectra is discussed below.

Before measurement of any branching ratios, a catalog of the potential "pump" transitions (transitions used to excite the ion from a ground or metastable state to the energy level of interest) and anticipated branches was compiled from the Kurucz Atomic Line Database [11, 12]. This catalog was used to identify all the possible branches from the level of interest that were accessible within the wavelength range of the Stilbene 3 dye-tuning curve. From these transitions, one with a large listed Einstein A-coefficient originating from a low-lying level was chosen as the pump transition. A transition other than the pump transition with a large listed branching ratio was chosen as the "normalization" transition.

In Fig. 1, the "normalization" monochromator coupled with a bialkali-photocathode photomultiplier tube (PMT) (Electron Tubes Ltd., 9235QB) was set to the wavelength of the normalization transition. Output from this PMT was analyzed by two lock-in amplifiers: one operating in "$2f$" mode provided the background-suppressed normalization signal, while the second, operating in "$1f$" mode, provided a derivative signal for dye-laser wavelength stabilization. The normalization signal was maximized by making minute corrections to the ion beam steering to optimize the overlap of the laser and the ion beam and was recorded concurrently with the branching ratio spectra on the data acquisition computer. Division of the branching ratio data by the normalization signal in software made this measurement relatively insensitive to laser power fluctuations, ion-beam current fluctuations, and steering/pointing instabilities in either beam. The derivative-shaped output of the $1f$-mode lock-in amplifier provided an error signal that was input to the scanning control of the dye laser to lock its wavelength to the pump transition. This wavelength lock would typically hold for 15–20 min before the correction signal reached its limit and had to be manually reset to centre range.

With the laser wavelength locked to the peak of the pump-transition resonance, the "branching ratio" monochromator (Fig. 1), coupled to a thermoelectrically-cooled trialkali PMT (Electron Tubes Ltd., 9658R), was scanned to record the spontaneous emission spectrum from 300–850 nm and the fluorescence from the decay branches was recorded. This signal was input to a third lock-in amplifier operating in $2f$ mode and its background-suppressed output was recorded on the data acquisition computer, which also controlled the scanning of the monochromator grating. A typical scan would step the monochromator grating 1 nm per step and would dwell for 2 s per step, taking from 5 to 15 min per scan.

A typical branching ratio spectrum with excellent SNR is shown in Fig. 4. The energy level at 26 540.119 cm^{-1} was excited by pumping the transition at 425.64 nm from the 3052.65 cm^{-1} metastable state. The LIF from 10 decay branches in the wavelength range 400–850 nm was recorded by scanning the monochromator in steps of 1 nm with a dwell time of 2 s per step, utilizing the 1200 groove/mm grating. The curve shown in Fig. 4 is a fit to the data of a model (see below) used to determine the relative line intensities. LIF from the transition at 441.76 nm was recorded as the normalization signal.

Fig. 4. A typical branching-ratio spectrum showing data points and the fit using symmetric Gaussians on a constant background. The energy level at 26 540.119 cm^{-1} was excited by pumping on the transition at 425.64 nm from the 3052.65 cm^{-1} lower state. The fluorescence from nine decay branches in the wavelength range 400–850 nm was recorded. The ion current was 81 nA and the laser power was 85 mW.

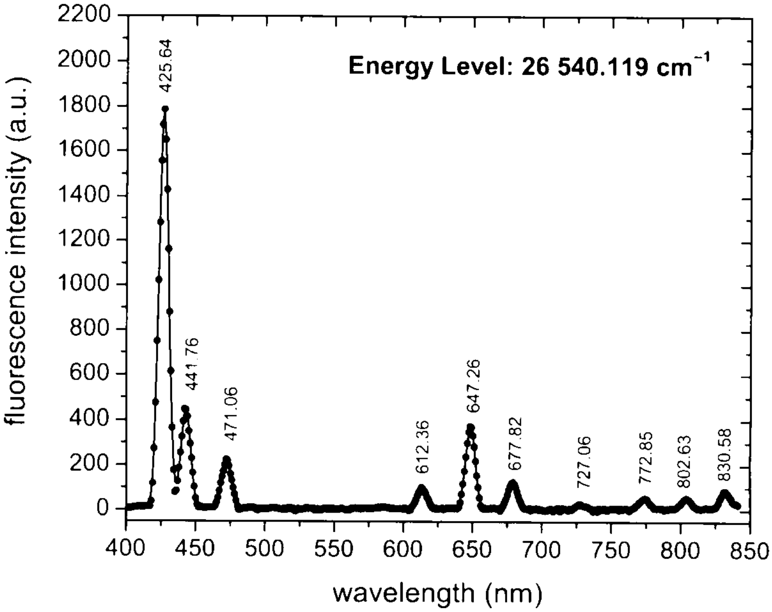

The Sm^+ ion-beam current was 81 nA and the laser power was 85 mW. This spectrum illustrates one of the advantages of the selective excitation mentioned earlier. The decay branch at 727.06 nm was heretofore unattributed to the 26 540.119 cm^{-1} level, but in this spectrum can unambiguously be assigned to it.

3. Data analysis

The calculation of branching ratios from a spectrum such as that shown in Fig. 4 consisted of two tasks: measuring the area under the line profile associated with a particular decay branch, and obtaining a proper spectral calibration of the detector system. For transitions from an upper state u to a set of lower states l, the relative intensities I_{ul} are obtained by dividing the areas S_{ul} of the observed spectral lines by the wavelength-dependent efficiency $\varepsilon(\lambda)$ of the fiber/monochromator/PMT system

$$I_{ul} = \frac{S_{ul}}{\varepsilon(\lambda_{ul})} \tag{1}$$

Branching ratios R_{ul} are then obtained as

$$R_{ul} = \frac{I_{ul}\,\lambda_{ul}}{\sum_l I_{ul}\,\lambda_{ul}} \tag{2}$$

The procedures and possible systematic errors associated with these tasks are described in the following paragraphs.

3.1. Line-profile fitting

To determine the areas under the emission peaks, a nonlinear least-squares fitting routine was used to fit a spectrum, using as parameters a constant background, peak line centres, peak widths (see below), and peak areas. The statistical uncertainties in the fitted areas ranged from ~0.2% to ~27% depending mainly on the peak size. To combine the relative intensities from spectra measured with different gratings so we could obtain a complete set of branching ratios, we employed a least-squares adjustment of $n-1$ multiplicative constants when the fitted areas from n spectra were being merged.

The actual shape of the line profile is primarily determined by the instrument response of the Czerny–Turner monochromator and is asymmetric about the line centre due to the formation of a curved image of the finite-height entrance slit on the exit slit of the monochromator [23]. To ensure that the intensity ratios were model-independent, the results of fitting several different line profiles were compared. These included symmetric and asymmetric Gaussians and triangular functions. The conclusion of this study was that the results were statistically insensitive to asymmetry and to the choice of Gaussian or triangular functions. For this reason and because Gaussian fitting is more robust, it was decided to use the symmetric Gaussian function in all line-profile fitting.

In fitting a spectrum it was necessary to use a wavelength-dependent width parameter $w(\lambda)$ because a Czerny–Turner scanning monochromator has a wavelength-dependent dispersion that causes the peaks to narrow toward longer wavelengths [23]. For the 2400 groove/mm grating a peak at 725 nm will have ~55% of the width of a peak at 400 nm. It should be noted that, even given this line narrowing, the total area under the peak does not systematically change as a function of wavelength, as can be seen from the fact that the area of the convolution of two functions is equal to the product of their individual areas.

We explored a number of simple models for $w(\lambda)$. They included an independent linewidth for each peak, linear and quadratic models, and a physical model that explicitly accounted for the diffraction of obliquely incident rays at the grating but did not include optical aberrations. The physical model was found to fit the highest SNR data, but required fairly nonrealistic parameters. The linear model gave a poor fit to the data. As for the independent linewidth model, it was found that small noisy peaks could not be fit with reasonable parameters. Our final choice was a simple quadratic function, $w(\lambda) = A\left(\lambda-\bar{\lambda}\right)^2 + B\left(\lambda-\bar{\lambda}\right) + C$, where $\bar{\lambda}$ is the mean wavelength of the scanned range. This function was completely adequate to describe the nonlinear dependence on wavelength and had the added advantage of being robust during the fitting of hundreds of spectra, some with poor SNR. Shifting the wavelength origin to $\bar{\lambda}$ improved the fitting procedure by avoiding correlations in the fitted parameters.

3.2. Efficiency calibration

An important source of uncertainty in the branching-ratio results comes from the uncertainty in the relative efficiency of our detector system (fiber array, monochromator, and PMT) as a function of wavelength. To measure this efficiency, a 200 W NIST-traceable quartz–tungsten–halogen (QTH) lamp (Oriel model 63355) was used as a standard illumination source with calibrated emission in the wavelength range 250–2500 nm. The uncertainty of the manufacturer's calibration within the wavelength range utilized to calibrate our system includes a 1.09–0.91% wavelength-dependent uncertainty in the NIST standard lamp plus a 1.5% uncertainty in the secondary-standard transfer calibration procedure. The manufacturer quotes a total (quadrature sum) uncertainty of 1.85% at 350 nm, 1.75% at 654.6 nm, and 1.85% at 900 nm. Although such calibrated QTH lamps are prone to spectral degradation with use, the very low-hour usage of our repeated efficiency calibrations over a period of several months resulted in no noticeable ageing effects. Nevertheless, data supplied by the manufacturer in which several lamps are compared over time suggest possible ageing effects as large as 3.5% change in output per 100 operating hours, particularly at the short-wavelength end of the spectrum. For the worst-case lamp tested, the differential change in the range 350–800 nm is 2.0%/100 h. Given an 87 h operating time for our calibration lamp, we have accordingly assigned 2% as our estimate of possible systematic

Fig. 5. Relative spectral efficiency versus wavelength calibration curves for the three gratings used in the branching-ratio experiment. A calibrated quartz–tungsten halogen lamp was used as a stable broadband emission source. The deviation of repeated measurements from the least-squares average is shown for each grating. The plotted relative efficiency scale is different for each of the three gratings to make their features more visible.

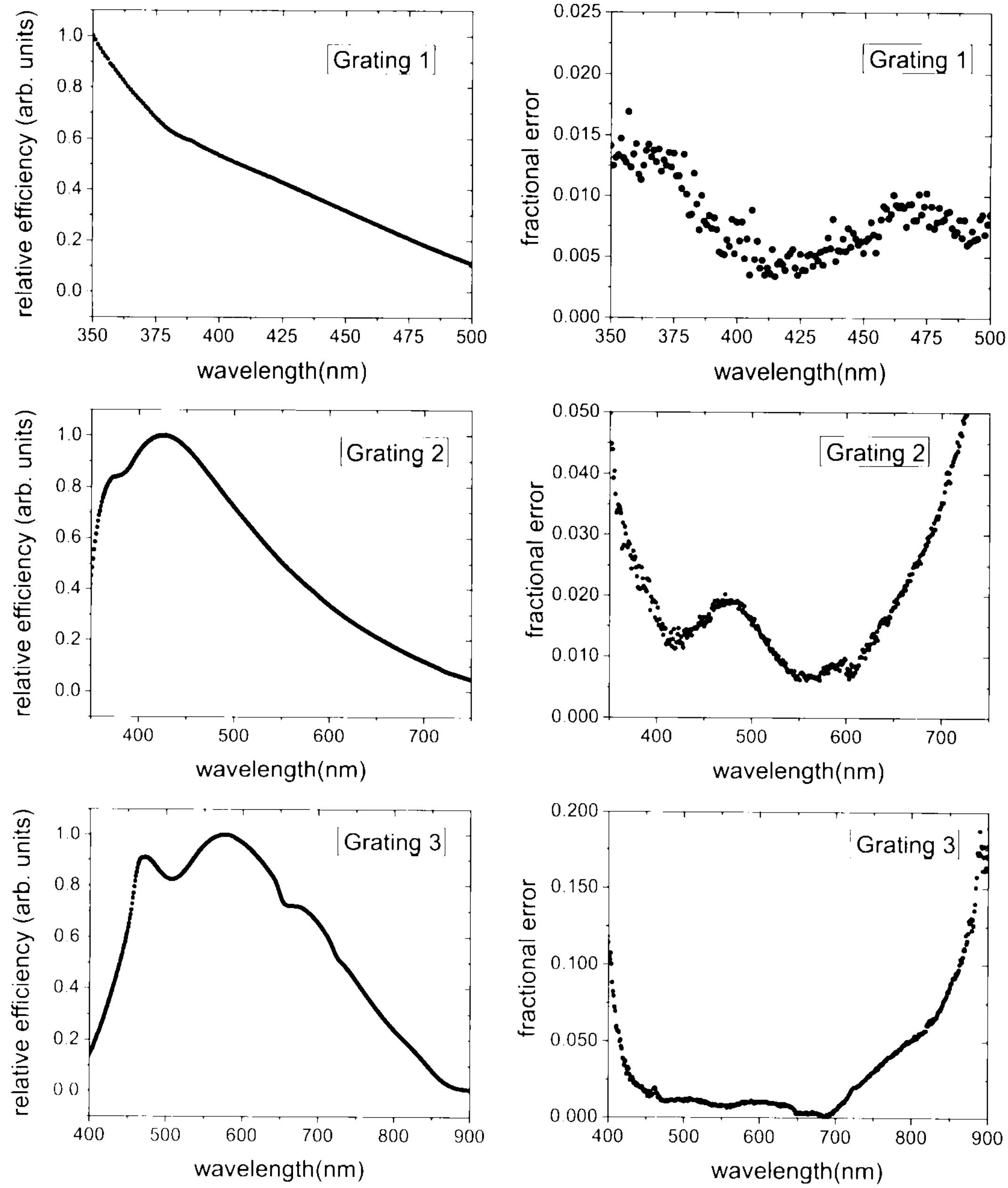

error from ageing. The NIST/transfer and ageing uncertainties have been added linearly, since they are systematic effects, to achieve a total lamp calibration uncertainty of 3.9%.

Initial calibrations were conducted on an isolated test bench using various input configurations. These experiments showed that slight differences in the way light is introduced to the monochromator could cause large changes in the response. A narrow cone of light entering the monochromator off-axis could lead to underestimates of the efficiency at long wavelengths, where some of the collimated calibration light could miss the highly tilted diffraction grating. As well, overfilling the entrance solid angle of the monochromator could lead to stray-light effects that were severely exaggerated when the intense long-wavelength continuum of the QTH lamp was present, but were absent in the actual BR measurement. Therefore, great care was taken to block paths by which stray light from the QTH continuum source could travel from the entrance slit to the exit slit of the monochromator.

The conclusion drawn from these initial calibrations was that measuring the relative spectral efficiency in situ was the best way to perform the calibration. This was done by decoupling one of the fiber bundles from its monochromator and illuminating the decoupled end of the bundle with the QTH lamp to transmit its light to the post-acceleration region. Some of the emergent light was collected by the other 80-fiber bundle, and transmitted to the test monochromator. Each grating in the monochromator was then scanned over its full wavelength range, and the resulting intensity curve was divided by the manufacturer-provided QTH lamp emission curve to produce a calibration curve of relative efficiency versus wavelength. The relative efficiency calibration curves of our system for the three gratings used in the experiment are shown in Fig. 5. Note that the relative efficiencies of the three gratings as presented in Fig. 5 cannot be compared directly to each other as different scales were used in plotting each grating to make the spectral dependence visible. Repeated calibrations spanning several months were rescaled with a least-squares procedure to minimize the residuals summed over wavelength, and showed very little change in the relative spectral efficiency of our system. The residuals provided an estimate of the uncertainty in the calibration due to misalignments and (or) changes in the light collection system. These deviations, with typical values less than 3%, are shown in Fig. 5 with their corresponding efficiency curves.

This calibration procedure most closely reproduced the actual conditions present during the experiment, with two minor differences. In the calibration procedure, the light passed through twice the length of optical fiber compared with that in the actual experiment. With a specified attenuation in the fiber of $\sim$10 dB/km throughout our wavelength range, the nominal attenuation in the additional length of input fiber was estimated to be $\sim$0.1%. We took 0.2% as a conservative estimate of the maximum uncertainty in the ratio of any two spectral components in our wavelength range due to fiber attenuation. The second difference is that the fraction of light reaching the fibers either directly or by scattering may be somewhat different in the calibration procedure and in the real experiment. However, any scattering must be from the colloidal graphite coating on the aluminum ring that holds the fibers, and the reflection coefficient from such a surface is fairly flat over the wavelength range of interest.

To obtain an empirical estimate of the uncertainty in our measurement of the relative detection efficiency, we examined the relative intensity of all spectral lines that were common to two or more scans, each taken with a different grating. This test exposed any scatter greater than that expected from the statistical uncertainty in the calibration shown in Fig. 5. Such excess scatter can only be due to systematic effects in our calibration. We found that the average magnitude of this excess was $\sim$3% and it is combined with the fiber attenuation uncertainty to derive a total uncertainty of 3.2%, which appears in Table 1 as "(systematic) efficiency calibration procedure".

3.3. Fiber geometry

As described above, two different fiber geometries were used to compensate for anisotropic excitation. To test the degree of compensation and the relative collection efficiency, several branching-ratio spectra for the same upper level were obtained with the roles of the two arrays switched. No statistical difference in the intensity ratios for different branches was found.

Table 1. Estimated uncertainties in the determination of relative intensities.

Source of uncertainty	Uncertainty (%)
Systematic:	
Total lamp calibration[a]	3.9
Efficiency calibration procedure[b]	3.2
Statistical:	
Fit of line profiles to data[c]	~0.2–5
Efficiency calibration procedure[d]	1.5

[a]NIST, transfer to Oriel lamp, lamp aging.
[b]Includes 0.2% for fiber attenuation effect.
[c]The range shown is from a sample of six spectra, and represents 70% of the distribution. Individual uncertainties for each fit were used in arriving at the total uncertainties for the BRs from that fit.
[d]The uncertainty shown is a sample mean. See Fig. 5.

3.4. Choice of pump transition

Because of the selectivity of excitation in the beam-laser method, the laser wavelength could be tuned to two or more different pump transitions sequentially and the branching ratios from the two spectra compared. As a check of any systematic errors connected with a particular pump transition, the branching-ratio spectrum from the 24 928.80 cm^{-1} level was acquired using three different pump transitions to populate this level. No statistically significant difference was found.

3.5. Unobserved branches

Obtaining branching ratios from relative intensities assumes that all radiative transitions that contribute to the decay of the level have been observed. Because of negligible detector response beyond 900 nm, we know that some branches seen in previous work have indeed been missed. The measurements of Meggers et al. [7] extend to 891.4 nm, while the HFR calculations of Xu et al. [14] go to 984.4 nm but do not consider levels beyond 27 695 cm^{-1}. Considering the level of agreement of our data with older data, we have not attempted to modify our branching ratios using these older data. Instead, in tabulating the relative intensities (see Table 2), we have listed data for all transitions not seen by us but present in the older data. These data give the reader an opportunity to gauge the effect of unobserved branches and to recalculate branching ratios from the relative intensities for relatively unambiguous cases. To illustrate the problem, consider the data for the level with energy 23 962.250 cm^{-1}. The data of ref. 6 include three levels beyond 750 nm that we did not observe, representing 3.5% of their total relative intensity. However, among the five levels that *are* common to this work and ref. 6, one of the strongest disagrees in its relative intensity by a factor of 1.6.

3.6. Summary of uncertainties

Estimates of the uncertainties in our determination of the relative intensities of radiative transitions in Sm II are summarized in Table 1. The total uncertainty was obtained by combining in quadrature the statistical uncertainty from the fitting and calibration procedures with the systematic uncertainty from the efficiency calibration (including lamp calibration). Repeated measurements of the relative intensities of branches from a single upper level taken over many months yielded deviations of less than 1% for the large branches (branching ratios larger than 10%) and less than 3% for the smaller branches. The excellent repeatability and self-consistency of these measurements confirms that the systematic uncertainty in the relative efficiency calibration dominates the error budget.

Table 2. Measured relative intensities in Sm II. To facilitate comparison, we have set the intensity of the strongest line observed in *our* work to 1. Branches that were observed but were too small to fit are indicated by the letter w.

Upper level energy (cm^{-1})	Lower level energy (cm^{-1})	Transition wavelength (nm)	Relative intensity		
			This work	MCS[a]	XSQGB[b]
21655.420	0.000	461.649[c]	0.08(1)	0.078	
	326.640	468.719	1	1	
	1518.290	496.457	0.14(2)	0.122	
	2003.230	508.707	0.072(9)	0.078	
	7135.060	688.499	0.016(3)		
	8578.700	764.507	0.08(1)	0.122	
	10371.510	885.974		0.070	
21702.330	0.000	460.651[c]	0.46(5)	0.426	0.7(3)
	326.640	467.690	1	1	1
	838.220	479.158	0.23(3)	0.338	0.11(6)
	1518.290	495.303	0.046(9)	0.066	
	2688.690	525.792	w		
	7135.060	686.281	0.07(3)	0.059	0.12(7)
	7524.860	705.150	0.21(5)	0.132	0.3(1)
	10873.300	923.190			0.03(2)
21904.119	0.000	456.407[c]	0.15(2)	0.128	
	326.640	463.316			0.2(1)
	838.220	474.568	1	1	1
	1518.290	490.400	w		
	2003.230	502.350	0.11(1)	0.128	
	2688.690	520.270	0.043(5)	0.128	
	7524.860	695.255	0.012(2)		
	8578.700	750.239	0.041(6)	0.049	
	9410.000	800.156	0.036(7)	0.040	0.05(3)
	10518.500	878.060			0.08(5)
	10743.400	895.754			0.08(5)
	10873.300	906.302			0.07(4)
22248.320	326.640	456.042[c]	0.25(3)	0.324	
	838.220	466.939	1	1	
	1489.160	481.581	0.52(5)	0.581	
	2003.230	493.809	0.13(1)	0.162	
	2688.690	511.115	0.015(2)		
	3499.120	533.208	0.009(2)		
	7135.060	661.488	0.009(2)		
	7524.860	679.001	0.074(8)	0.081	
	8046.000	703.916	0.17(2)	0.122	
	10873.300	878.878		0.031	
22875.410	838.220	453.651[c]	0.22(2)	0.245	1.2(5)
	1489.160	467.459	1	1	1
	2237.970	484.421	0.43(4)	0.282	0.11(6)
	2688.690	495.237	0.16(2)	0.109	0.07(4)
	3499.120	515.951	0.019(2)		
	4386.030	540.701	0.005(1)		
	7524.860	651.263	0.006(2)		
	8046.000	674.150	0.061(7)	0.050	0.16(7)

Table 2. (*continued*).

Upper level energy (cm^{-1})	Lower level energy (cm^{-1})	Transition wavelength (nm)	Relative intensity		
			This work	MCS[a]	XSQGB[b]
	8679.230	704.221	0.14(1)	0.082	0.3(1)
	11395.400	870.840			0.03(1)
	11659.800	891.370			0.02(1)
23177.490	0.000	431.332	0.053(6)		
	326.640	437.498[c]	0.38(4)	0.681	0.13(8)
	838.220	447.517	0.12(1)	0.160	
	1518.290	461.568	1	1	1
	2003.230	472.139	w	0.062	
	2688.690	487.936	w		
	7524.860	638.694	0.013(6)		0.09(5)
	8578.700	684.800	0.017(8)		
	10873.300	812.508		0.019	0.013(8)
23260.949	838.220	445.851[c]	1	1	
	1489.160	459.181	0.32(3)	0.290	
	2237.970	475.537	0.048(5)	0.040	
	2688.690	485.956	0.11(1)	0.085	
	3499.120	505.885	0.016(3)		
	8046.000	657.067	0.056(6)	0.035	
	8679.230	685.601	0.13(2)	0.075	
	12045.170	891.356		0.095	
23646.900	1489.160	451.183[c]	0.59(6)	0.903	
	2237.970	466.964	1	1	
	3052.650	485.437	0.17(2)	0.194	
	3499.120	496.194	0.22(2)	0.274	
	4386.030	519.043	w		
	8679.230	667.922	0.079(9)	0.113	
	9406.630	702.040	0.22(3)	0.145	
	12045.170	861.704		0.037	
	12232.340	875.834		0.048	
23659.990	0.000	422.535	0.22(4)	2.273[c]	
	326.640	428.451	0.05(3)	0.080	
	1518.290	451.510[c]	1	1	
	7135.060	604.979	0.009(5)		
	8578.700	662.890	0.035(9)	0.045	
	10518.500	760.739	0.02(1)	0.052[c]	
23842.199	326.640	425.131	0.011(2)		
	838.220	434.585[c]	0.47(5)	0.949	
	1489.160	447.241	0.52(5)	0.797	
	2003.230	457.769	1	1	
	2688.690	472.603	0.21(2)	0.220	
	3499.120	491.430	0.032(4)	0.024	
	7135.060	598.381	0.012(4)		
	7524.860	612.676	w		
	8046.000	632.889	0.016(5)		
	8578.700	654.977	0.036(7)	0.031	
	9410.000	692.704	0.029(9)	0.027	
	11155.300	787.998		0.017	

Table 2. (*continued*).

Upper level energy (cm^{-1})	Lower level energy (cm^{-1})	Transition wavelength (nm)	Relative intensity		
			This work	MCS[a]	XSQGB[b]
	11395.400	803.199		0.027	
	11659.800	820.631		0.010	
	11798.600	830.088		0.017	
23962.250	326.640	422.971	1	1	
	838.220	432.329[c]	0.82(8)	0.797	
	2003.230	455.266	0.89(9)	0.554	
	2688.690	469.936	0.19(2)	0.162	
	8578.700	649.866	0.11(2)	0.047	
	10743.400	756.287		0.026	
	10873.300	763.793		0.031	
	11798.600	821.896		0.035	
24013.561	0.000	416.314	0.36(4)	0.421	
	326.640	422.055	0.09(1)		
	838.220	431.372	0.26(3)	0.474[c]	
	2003.230	454.205	1	1	
24194.381	838.220	428.032[c]	0.57(6)	0.500	
	1489.160	440.304	0.56(6)	4.500[c]	
	2003.230	450.504	1	1	
	2688.690	464.863	0.09(1)		
	3499.120	483.068	0.05(1)		
	7135.060	586.027	0.08(3)	0.078	
24221.811	326.640	418.377	0.80(9)	1.432	
	1518.290	440.337[c]	0.63(7)	1.108	
	2003.230	449.948	1	1	
	8578.700	639.082	0.08(1)	0.068	
	10371.510	721.807	w	0.070	
	11047.300	758.833	w	0.062	
24257.369	1489.160	439.086[c]	1	1	1
	2237.970	454.018	0.14(1)	0.181	1.9(8)
	3052.650	471.461	0.077(9)	0.047	0.3(1)
	3499.120	481.602	0.08(1)	0.053	0.15(9)
	4386.030	503.098	0.013(4)		
	8679.230	641.748	0.045(6)	0.018	0.2(1)
	9406.630	673.181	0.12(2)	0.075	0.3(1)
	10180.700	710.200	0.010(2)		
	10960.160	751.831	w		
	11395.400	777.272	w		
	12045.100	818.628	w		0.06(4)
	12232.340	831.370	w		0.10(6)
	12789.810	871.786	w	0.019	0.02(1)
	12841.600	875.741	w		0.04(2)
24429.520	0.000	409.225	1	1	1
	326.640	414.771	0.30(3)	0.320	0.000(0)
	838.220	423.766[c]	0.68(7)	0.500	0.13(8)
	1518.290	436.345	0.32(3)	0.220	
	2003.230	445.780	0.033(4)		0.000(0)
	2688.690	459.835	0.19(2)	0.090	0.11(6)

Table 2. (*continued*).

Upper level energy (cm^{-1})	Lower level energy (cm^{-1})	Transition wavelength (nm)	Relative intensity: This work	Relative intensity: MCS[a]	Relative intensity: XSQGB[b]
	7524.860	591.389	0.021(4)		
	8578.700	630.708	0.065(8)	0.035	
	9410.000	665.616	0.051(6)	0.027	0.10(4)
	10371.510	711.143	0.009(2)		
	10518.500	718.657			0.02(1)
	10743.400	730.466	0.014(3)		
	10873.300	737.466			0.06(4)
	11155.300	753.133	0.009(3)		
	11798.600	791.490	0.048(8)	0.026	
24582.590	326.640	412.154	0.09(1)	0.067	
	838.220	421.034	0.38(4)	0.367	
	1489.160	432.902[c]	1	1	
	2003.230	442.758	0.16(2)	0.100	
	2688.690	456.620	0.66(7)	0.261	
	3499.120	474.173	0.050(5)	0.028	
	8578.700	624.675	0.033(4)	0.025	
	9410.000	658.902	0.013(2)		
	10180.700	694.162	0.025(3)	0.009	
	10518.500	710.835	0.005(1)		
	11155.300	744.547	0.024(3)		
	11659.800	773.614[d]	0.028(4)	0.017	
	11798.600	782.013[d]		0.009	
24588.000	2237.970	447.301[c]	0.71(8)	0.705	0.9(3)
	3052.650	464.223	1	1	1
	3909.620	483.462	0.08(1)	0.085	0.07(3)
	4386.030	494.863	0.26(3)	0.193	0.07(4)
	8679.230	628.410			0.08(3)
	9406.630	658.520	0.053(7)	0.045	0.03(1)
	10214.380	695.527	0.18(2)	0.136	0.27(8)
	12789.810	847.355			0.02(1)
	12841.600	851.091			0.05(3)
	13466.500	898.913			0.03(1)
	13604.500	910.207			0.011(6)
24685.529	0.000	404.981	1	1	
	326.640	410.412	0.63(8)	0.407	
	838.220	419.216	0.7(1)	0.271	
	1518.290	431.523	0.11(2)		
	2003.230	440.749[c]	0.24(5)	0.102	
	2688.690	454.483	0.44(7)	0.169	
	7135.060	569.627	0.07(2)	0.037	
			0.031		
24689.840	1489.160	430.901	0.51(5)	0.677	
	2237.970	445.272[c]	1	1	
	2688.690	454.394	0.79(8)	0.623	
	3499.120	471.773	0.26(3)	0.162	
	4386.030	492.381	0.032(3)	0.046	
	8679.230	624.413	w	0.019	

Table 2. (*continued*).

Upper level energy (cm^{-1})	Lower level energy (cm^{-1})	Transition wavelength (nm)	Relative intensity This work	MCS[a]	XSQGB[b]
	9410.000	654.276	0.046(5)	0.038	
	10960.160	728.149	0.029(3)	0.020	
	11659.800	767.246		0.006	
	11798.600	775.507		0.018	
	12232.340	802.509		0.018	
	12987.860	854.322		0.018	
24848.471	326.640	407.685	0.31(3)	0.075	
	838.220	416.371	0.33(3)	0.083	
	1489.160	427.974[c]	1	1[c]	
	2003.230	437.605	0.057(6)		
	3499.120	468.267	0.36(4)	0.063	
	7135.060	564.388	0.031(4)		
	7524.860	577.087	0.028(4)		
	8046.000	594.986	0.004(4)		
	8578.700	614.467	0.018(3)		
	9410.000	647.554	0.017(3)		
	10518.500	697.646	0.007(5)		
	10873.300	715.358	0.009(6)		
	11155.300	730.090	0.030(8)		
	11395.400	743.120	0.019(8)		
	11659.800	758.018	0.029(9)		
24928.801	326.640	406.354	1	1	
	838.220	414.983	0.69(7)	1.446	
	1489.160	426.508	0.47(5)	0.893	
	2003.230	436.072[c]	0.65(7)	1	
	2688.690	449.512	0.034(5)	0.043	
	3499.120	466.512	0.14(1)	0.134	
	8578.700	611.448	w	0.032	
	10180.700	677.866	w	0.071	
	11798.600	761.393		0.021	
25055.539	0.000	399.001	0.90(9)	2.027[c]	
	326.640	404.271	1	1	
	838.220	412.811	0.057(8)	0.039	
	1518.290	424.739	0.10(1)	0.068	
	2003.230	433.674	0.11(1)	0.061	
	2688.690	446.965[c]	0.19(2)	0.122	
	9410.000	638.983	0.08(2)	0.039	
	10518.500	687.708		0.016	
	10873.300	704.913	0.06(6)	0.018	
25175.320	326.640	402.322	1	1	
	838.220	410.779	0.072(9)	0.068	
	1489.160	422.069	0.041(7)		
	2003.230	431.433	0.042(7)		
	2688.690	444.584[c]	0.08(1)	0.040	
	3499.120	461.207	0.025(5)		
	7135.060	554.162	w		
	8046.000	583.633	0.09(1)	0.051	
	10180.700	666.722	0.10(2)	0.019	

Table 2. (*continued*).

Upper level energy (cm^{-1})	Lower level energy (cm^{-1})	Transition wavelength (nm)	Relative intensity		
			This work	MCS[a]	XSQGB[b]
25178.449	0.000	397.053	0.44(4)	0.740	
	326.640	402.272	0.048(6)	0.090	
	838.220	410.727	0.18(2)	0.810[c]	
	1518.290	422.532[c]	1	1[c]	
	2003.230	431.374	0.047(6)	0.180[c]	
25304.090	838.220	408.617		0.045	
	1489.160	419.786	0.033(4)	0.030	
	2237.970	433.414	0.9(1)	0.867	
	2688.690	442.052[c]	1	1	
	3499.120	458.483	0.53(6)	0.373	
	4386.030	477.923	0.016(3)		
	8046.000	579.278	w		
	8679.230	601.343	w		
	9410.000	628.991	0.023(5)	0.017	
	11659.800	732.706	1.2(2)	0.009	
	12232.340	764.798		0.013	
	12987.860	811.714		0.006	
25361.449	0.000	394.188	1	1	
	326.640	399.331	0.87(9)	0.569	
	838.220	407.662	0.30(3)	0.215	
	2003.230	427.994	0.57(6)	0.185	
	2688.690	440.934[c]	0.68(7)	0.400	
	9410.000	626.729	0.13(2)	0.077	
	10518.500	673.535	w		
	10873.300	690.029		0.008	
	11047.300	698.417	w	0.010	
25385.359	2237.970	431.893[c]	1	1	1
	3052.650	447.648			0.03(2)
	3909.620	465.511	0.11(2)	0.079	0.04(2)
	4386.030	476.073	0.014(5)		
	5317.560	498.172	0.009(5)	0.024	
	9406.630	625.659	0.026(3)	0.024	0.018(9)
	10214.380	658.971	0.082(9)	0.058	0.07(2)
	10960.160	693.040	0.014(2)	0.008	0.02(1)
	11791.050	735.399	0.003(1)		0.017(9)
	12045.100	749.408	0.007(2)		0.008(4)
	12789.810	793.713[d]	0.012(3)	0.010	
	12841.600	796.990[d]			
	13466.500	838.776	0.014(5)	0.010	0.04(1)
	13604.500	848.601	0.031(8)	0.024	0.07(2)
25417.141	326.640	398.445	0.08(1)		
	838.220	406.738	0.42(4)		
	1489.160	417.803[c]	1	1[c]	
	2003.230	426.976	0.25(3)	0.080	
	2688.690	439.854	0.026(9)		
	3499.120	456.118	0.25(3)	0.041	
	7524.860	558.746	w		

Table 2. (*continued*).

Upper level energy (cm^{-1})	Lower level energy (cm^{-1})	Transition wavelength (nm)	Relative intensity		
			This work	MCS[a]	XSQGB[b]
	8578.700	593.715	w		
	9410.000	624.549	w		
	10518.500	671.017	w		
	11155.300	700.979	w		
	11395.400	712.982	w		
	11659.800	726.685	w		
	11798.600	734.091	w		
25552.801	326.640	396.302		2.679	
	838.220	404.505	1	1	
	1518.290	415.951	0.37(4)	0.179	
	2003.230	424.517[c]	0.71(7)	0.214	
	2688.690	437.244	0.058(7)		
	8578.700	588.970	w		
	9410.000	619.300	w		
	10743.400	675.061	w		
	11047.300	689.204	w		
25565.971	838.220	404.290	1	1	
	1489.160	415.220	0.9(1)	1.364	
	2237.970	428.549	0.61(6)	0.057	
	2688.690	436.992[c]	0.19(2)	0.239	
	4386.030	472.013	0.08(1)	0.040	
	9410.000	618.795	w	0.025	
	10180.700	649.793	0.04(2)		
	10960.160	684.470	0.09(2)	0.063	
	11395.400	705.493	w	0.018	
	11798.600	726.155		0.010	
	12045.170	739.398		0.015	
	12987.860	794.813		0.018	
25597.699	1489.160	414.674	0.045(9)	0.089	
	2237.970	427.967[c]	0.40(4)	0.667[c]	
	3052.650	443.432	1	1	
	3499.120	452.391	0.44(5)	0.361	
	4386.030	471.307	0.15(2)	0.150	
	5317.560	492.956	0.023(8)	0.016	
	10180.700	648.455	0.027(5)	0.019	
	10960.160	682.986	0.017(5)	0.015	
	11395.400	703.918	w		
	11791.050	724.089	0.022(9)	0.033	
	12045.170	737.666		0.014	
	12841.600	783.723		0.014	
	12987.860	792.813		0.050	
	13466.500	824.094		0.009	
	14115.000	870.636		0.007	
25664.971	3052.650	442.113[c]	1	1	
	3909.620	459.528	0.85(9)	0.583	
	5317.560	491.326	0.27(3)	0.365	
	9406.630	614.899	0.005(3)		

Table 2. *(continued)*.

Upper level energy (cm^{-1})	Lower level energy (cm^{-1})	Transition wavelength (nm)	Relative intensity This work	MCS[a]	XSQGB[b]
	10214.380	647.046	0.043(5)	0.019	
	11094.060	686.110	0.21(2)	0.125[c]	
	11791.050	720.578	0.005(4)		
	13466.500	819.550	0.03(1)	0.020	
	13604.500	828.927	w	0.020	
	14084.550	863.289	w	0.024	
25790.150	838.220	400.657	0.25(3)	0.306	
	1489.160	411.390	0.60(6)	0.661	
	2237.970	424.470[c]	1	1	
	2688.690	432.751	0.11(1)	0.073	
	3499.120	448.486	0.022(3)		
	4386.030	467.069	0.12(1)		
	7524.860	547.335	0.026(3)		
	8679.230	584.260	0.044(5)	0.035	
	9410.000	610.326	0.043(6)		
	10180.700	640.461	0.015(4)		
	10960.160	674.124	0.09(1)		
25939.869	3052.650	436.802[c]	0.40(4)	0.704	
	3909.620	453.794	1	1	
	5317.560	484.776	0.33(3)	0.197	
	10214.380	635.735	0.022(7)		
	11094.060	673.405	0.13(2)	0.099	
	13466.500	801.488		0.027	
	14084.550	843.271		0.042	
25980.320	326.640	389.697	1	1	
	838.220	397.627	0.54(6)	0.600	
	1489.160	408.195	0.075(8)	0.081	
	2003.230	416.947	0.65(7)	0.506	
	2688.690	429.218[c]	0.41(4)	0.219	
	3499.120	444.691	0.048(6)	0.028	
	9410.000	603.322	0.021(4)	0.011	
	10180.700	632.752	0.09(1)	0.044	
	10873.300	661.761	0.011(4)	0.007	
	11047.300	669.472	0.015(4)	0.007	
	11395.400	685.451	0.022(5)	0.009	
	12566.800	745.311	0.08(2)	0.016	
26046.350	3052.650	434.780	0.61(6)	0.688	
	3499.120	443.389[c]	1	1	
	4386.030	461.544	0.27(3)	0.181	
	5317.560	482.286	0.006(1)		
	8046.000	555.391	0.003(1)		
	8679.230	575.641	0.004(1)		
	9406.630	600.806	0.006(1)		
	10180.700	630.118	0.014(2)	0.014	
	12232.340	723.703	0.017(2)	0.008	
	12789.810	754.137[d]	0.029(3)	0.014	
	12841.600	757.095[d]		0.014	

Table 2. (*continued*).

Upper level energy (cm⁻¹)	Lower level energy (cm⁻¹)	Transition wavelength (nm)	Relative intensity: This work	MCS[a]	XSQGB[b]
	12987.860	765.575	0.011(2)	0.006	
26086.631	838.220	395.953	0.74(8)	0.902	
	1489.160	406.431	0.64(7)	0.683	
	2237.970	419.193[c]	1	1	
	3499.120	442.598	0.15(2)	0.085	
	4386.030	460.688	0.25(3)	0.110	
	8679.230	574.309	0.02(1)		
	10180.700	628.523	0.03(2)		
	11659.800	692.962	0.06(3)	0.029	
	12045.170	711.980	0.15(4)	0.063	
26159.600	838.220	394.811	1	1	
	1489.160	405.229	0.027(6)		
	2688.690	425.939[c]	0.044(7)	0.068	
	3499.120	441.173	0.039(6)		
	4386.030	459.144	0.012(5)		
	8046.000	551.918	0.009(6)		
	8679.230	571.912	0.025(8)	0.019	
	11659.800	689.475	0.05(3)		
26190.920	326.640	386.524	0.35(4)	0.432	
	838.220	394.324	0.89(9)	0.838	
	1489.160	404.715	1	1	
	2003.230	413.317	0.13(1)	0.135	
	2688.690	425.372[c]	0.11(1)	0.081	
	3499.120	440.564	0.09(1)	0.047	
	9410.000	595.750	0.06(1)	0.030	
	10180.700	624.429	0.08(1)		
	10873.300	652.663	0.06(2)	0.018	
	11155.300	664.904	w	0.027	
	11798.600	694.624	0.11(3)		
26214.051	326.640	386.179	0.46(5)		
	838.220	393.964	0.12(1)	0.179	
	1489.160	404.337	0.18(2)		
	2003.230	412.922	1	1	
	2688.690	424.954[c]	0.85(9)	0.750	
	3499.120	440.116	0.48(5)		
26357.900	326.640	384.045	0.69(8)	0.909	1
	838.220	391.744	0.9(1)	1.409	
	1489.160	401.998	0.49(6)	0.636	0.21(9)
	2003.230	410.483	w		
	2688.690	422.371	0.43(5)	0.341	0.3(1)
	3499.120	437.346[c]	1	1	
	9410.000	589.880	w		
	10180.700	617.983	0.07(2)	0.050	0.07(4)
	10518.500	631.163			0.02(1)
	10873.300	645.625		0.023	0.03(2)
	11155.300	657.601			0.016(9)
	11395.400	668.153	0.09(2)	0.039	0.07(4)
	14667.960	855.201			0.013(7)

Table 2. (*continued*).

Upper level energy (cm^{-1})	Lower level energy (cm^{-1})	Transition wavelength (nm)	Relative intensity		
			This work	MCS[a]	XSQGB[b]
26505.529	2237.970	411.957	0.036(4)	0.052	
	3052.650	426.267	0.24(2)	0.448	
	3909.620	442.434[c]	1	1	
	4386.030	451.963	0.30(3)	0.303	
	5317.560	471.834	0.084(9)	0.066	
	10960.160	643.101	0.010(2)	0.008	
	11791.050	679.415	0.045(5)	0.033	
	12789.810	728.890	w	0.006	
	12841.600	731.653	0.004(2)		
	13466.500	766.717	w	0.007	
	13604.500	774.919	0.009(3)	0.010	
	14084.550	804.868[d]	0.043(7)	0.014	
	14115.000	806.846[d]		0.016	
26540.119	3052.650	425.639[c]	1	1	
	3909.620	441.758	0.16(2)	0.181	
	5317.560	471.065	0.045(5)	0.029	
	10214.380	612.360	0.014(1)	0.010	
	11094.060	647.235	0.063(7)	0.021	
	11791.050	677.822	0.020(2)	0.010	
	12789.810	727.056	0.004(1)		
	13604.500	772.847	0.014(2)	0.014	
	14084.550	802.633	0.019(2)	0.011	
	14503.670	830.582	0.044(5)	0.019	
26565.609	1489.160	398.668	1	1	
	2237.970	410.939	0.58(6)	0.554	
	3052.650	425.178[c]	0.45(5)	0.338	
	3499.120	433.408	0.050(6)		
	4386.030	450.739	0.028(5)		
	5317.560	470.500	0.032(5)		
	8046.000	539.819	0.041(7)		
	8679.230	558.930	0.024(6)		
	10960.160	640.625	0.11(2)	0.016	
	11395.400	659.005	w		
	11791.050	676.652	0.07(2)	0.019	
	12045.100	688.495	0.06(2)		
	12232.340	697.485	0.05(2)		
	12789.810	725.711	0.10(3)	0.012	
26599.080	0.000	375.846	0.59(7)	0.563	
	838.220	388.076	1	1	
	1518.290	398.599	0.24(3)	0.188	
	2003.230	406.458	0.84(9)	1.750[c]	
	2688.690	418.110[c]	0.77(8)	0.663	
	7135.060	513.626	0.06(2)	0.000	
	10518.500	621.696	0.10(5)	0.000	
	10743.400	630.514	0.10(5)	0.016	
	10873.300	635.723	0.16(5)	0.036	
	11047.300	642.836	0.22(6)	0.028	
	11798.600	675.467	0.09(7)	0.021[c]	

Table 2. (*continued*).

Upper level energy (cm^{-1})	Lower level energy (cm^{-1})	Transition wavelength (nm)	Relative intensity: This work	MCS[a]	XSQGB[b]
26723.869	326.640	378.720	0.35(4)	0.485	
	838.220	386.205	1	1	
	2003.230	404.406	0.46(5)	0.364	
	2688.690	415.940[c]	0.37(4)	0.152	
26820.811	1489.160	394.651	0.71(7)	0.617	
	2237.970	406.673	1	1	
	3052.650	420.612	1	0.815	
	3499.120	428.665[c]	0.46(5)	0.432	
	4386.030	445.611	0.13(1)	0.111	
	5317.560	464.916	0.035(6)		
	9406.630	574.086	0.033(8)		
	10180.700	600.792	0.035(9)		
	10960.160	630.317	0.07(1)	0.036	
	11791.050	665.163	w	0.025	
	12789.810	712.511	w	0.028	
26828.289	3052.650	420.480	0.022(3)	0.042	0.14(5)
	3909.620	436.203	0.54(5)	0.675	0.04(1)
	4386.030	445.463	1	1	1
	5317.560	464.754	0.15(2)	0.075	
	9406.630	573.839			0.008(4)
	10214.380	601.739		0.015	0.02(1)
	11791.050	664.832			0.009(5)
	12789.810	712.132			0.006(3)
	13466.500	748.197	0.67(9)	0.022	
	13604.500	756.005	0.25(5)	0.010	0.010(5)
	14084.550	784.483[d]	0.8(1)	0.008	
	14115.000	786.362[d]		0.016	0.002(1)
	15897.540	914.599			0.003(1)
	16615.500	978.896			0.04(1)
26880.600	3052.650	419.557	0.020(2)		
	3909.620	435.210[c]	0.80(8)	0.789	
	4386.030	444.427	1	1	
	5317.560	463.627	0.18(2)	0.127	
	8679.230	549.257	0.012(2)		
	9406.630	572.122	0.018(3)		
	10960.160	627.950	0.015(2)	0.014	
	11791.050	662.527	0.014(2)	0.008	
	12045.100	673.876	0.003(1)		
	12841.600	712.105	0.013(2)		
	13466.500	745.279	0.026(4)		
	14084.550	781.276		0.011	
	14115.000	783.140	0.043(6)	0.014	
26974.670	326.640	375.156	0.37(4)	0.762	
	838.220	382.499	0.34(4)		
	1489.160	392.269	0.31(3)	0.429	0.9(6)
	2003.230	400.344	0.90(9)	1.333	6.4(38)
	2688.690	411.644	0.74(8)	0.905	2.4(14)

Table 2. (*continued*).

Upper level energy (cm⁻¹)	Lower level energy (cm⁻¹)	Transition wavelength (nm)	Relative intensity		
			This work	MCS[a]	XSQGB[b]
	3499.120	425.855[c]	1	1	1
	8046.000	528.152	w		0.3(2)
	8578.700	543.447	w		
	11798.600	658.750	w		0.015(8)
	14667.960	812.342			0.08(4)
27107.619	838.220	380.563	0.30(3)	0.516	
	1489.160	390.233	0.06(1)	0.105	
	2237.970	401.983	0.15(2)	0.194	
	2688.690	409.403	0.34(4)	0.468	
	3499.120	423.457[c]	1	1	
	4386.030	439.987	0.12(2)	0.145	
	8679.230	542.491	0.020(5)		
	10960.160	619.122	0.025(8)		
	12045.100	663.721	0.05(1)		
	12566.800	687.529	w	0.016	
27165.350	326.640	372.490	1	1	1
	838.220	379.729	0.67(8)	1	
	1489.160	389.356			0.5(2)
	2003.230	397.310	0.16(3)		1.3(6)
	2688.690	408.437	0.64(8)	0.524	0.4(2)
	3499.120	422.424[c]	0.22(3)	0.119	
	7524.860	509.010	0.12(2)		0.3(2)
	8046.000	522.885	0.24(3)	0.143	
	8578.700	537.871	0.04(1)		
	14667.960	799.947			0.04(2)
27188.301	838.220	379.398	1	1	
	1489.160	389.008	0.5(2)	0.381	
	2237.970	400.683	0.07(4)	0.056	
	2688.690	408.055	0.2(1)	0.150	
	3499.120	422.015	0.2(1)	0.113	
	4386.030	438.430[c]	0.3(1)	0.181	
	8679.230	540.126	0.02(1)		
	10180.700	587.810	0.04(3)	0.008	
	10960.160	616.043	0.08(6)	0.014	
	11395.400	633.021	0.04(4)		
	12045.170	660.183	0.2(1)	0.025	
	12232.340	668.445	0.07(6)		
27263.250	3909.620	428.079[c]	1	1	
	11094.060	618.289	0.013(1)	0.013	
	12045.100	656.929	0.12(1)	0.064	
	14084.550	758.591	0.007(1)	0.014	
	14503.670	783.509	0.020(2)	0.018	
27284.689	326.640	370.841	0.48(5)	0.436	0.4(1)
	838.220	378.015	0.045(6)		
	1489.160	387.554	0.45(5)	0.509	
	2688.690	406.455	0.77(8)	1.273[c]	1.4(2)
	3499.120	420.305[c]	1	1	1

Table 2. (*continued*).

Upper level energy (cm⁻¹)	Lower level energy (cm⁻¹)	Transition wavelength (nm)	Relative intensity This work	MCS[a]	XSQGB[b]
	8046.000	519.642	0.015(4)		0.02(1)
	11047.300	615.692	0.033(8)	0.013	0.02(1)
	11155.300	619.815	0.043(8)	0.009	
	11395.400	629.181	0.06(1)	0.045	0.015(8)
	11659.800	639.828	0.043(9)		
	11798.600	645.562	0.06(1)	0.013	0.08(2)
	12566.800	679.258	0.05(1)	0.013	
	12987.860	699.263			0.013(7)
	14667.960	792.380			0.010(5)
	16078.000	892.059			0.006(3)
	17005.300	972.534			0.014(7)
27309.730	1489.160	387.178	1	1	
	2237.970	398.742	0.48(5)	0.463	
	3052.650	412.135	0.72(8)	0.513	
	4386.030	436.107[c]	0.50(5)	0.275	
	5317.560	454.580	0.11(1)	0.036	
	10180.700	583.643	0.11(2)		
	10960.160	611.468	0.15(3)		
	12232.340	663.062	0.11(4)	0.018	
	12789.810	688.519[d]	0.46(8)	0.034	
	12841.600	690.984[d]		0.018	
27464.199	838.220	375.466	0.057(8)		
	1489.160	384.876	0.18(2)	0.865	1.1(5)
	2237.970	396.301	1		1.1(5)
	2688.690	403.510	0.93(9)	1	1
	3499.120	417.156[c]	0.55(6)	0.554	0.3(2)
	4386.030	433.189	0.028(4)		
	8679.230	532.193	0.023(5)		
	9410.000	553.734	0.014(4)		
	10180.700	578.426			0.2(1)
	10873.300	602.573			0.12(7)
	10960.160	605.745			0.14(8)
	11395.400	622.152			0.15(9)
	11659.800	632.560	0.07(1)	0.024	0.011(7)
	12045.100	648.370	0.030(9)		0.3(1)
	12232.340	656.337	0.05(7)		0.08(5)
	12566.800	671.073	w		
	15242.950	818.022			0.03(2)
27695.961	3909.620	420.291[c]	0.078(8)	0.295	0.12(4)
	5317.560	446.734	1	1	1
	11094.060	602.174	0.005(1)		0.013(4)
	11791.050	628.563			0.006(3)
	13466.500	702.574			0.003(2)
	14084.550	734.475			0.010(5)
	14503.670	757.810	0.017(3)	0.009	0.017(5)
	16615.500	902.242			0.002(1)
	17391.890	970.224			0.04(1)

Table 2. (*continued*).

Upper level energy (cm^{-1})	Lower level energy (cm^{-1})	Transition wavelength (nm)	Relative intensity This work	MCS[a]	XSQGB[b]
28072.330	838.220	367.082	1	1	
	1489.160	376.071	0.64(7)	0.864	
	2688.690	393.843	w	0.013	
	3499.120	406.832	0.31(3)	0.323	
	4386.030	422.066[c]	0.62(6)	0.336	
	8046.000	499.203	0.09(1)	0.032	
	8679.230	515.504	0.24(3)	0.164	
	11395.400	599.465	0.04(1)	0.011	
	12045.170	623.768		0.013	
	12566.800	644.753		0.003	
	13777.050	699.339		0.006	
28151.400	2237.970	385.791	0.45(6)	0.649	
	3052.650	398.314	1	1	
	3909.620	412.395	0.81(9)	0.959	
	4386.030	420.662	0.57(7)	0.365	
	5317.560	437.824[c]	0.9(1)	1.189	
	11791.050	611.065	0.12(2)	0.061	
	13604.500	687.242	0.11(3)	0.036	
	14115.000	712.237	w	0.016	
28191.961	1489.160	374.387	1		
	2237.970	385.188	0.38(5)	1	
	3499.120	404.861	0.11(2)	0.500	
	4386.030	419.945	0.37(4)	0.643	
	5317.560	437.047[c]	0.13(3)	0.107	
	8679.230	512.344	w		
	9406.630	532.183	0.06(1)		
	10180.700	555.054	0.04(1)		
	10960.160	580.162	w	0.021	
	12045.100	619.147	w		
	12232.340	626.408	w		
	12789.810	649.081	0.21(4)	0.069	
28256.320	838.220	364.619	0.011(1)		
	1489.160	373.486	0.039(4)		
	2237.970	384.235	0.15(2)	0.270	
	2688.690	391.009	0.063(8)	0.090	
	3499.120	403.809	0.11(1)	0.150	
	4386.030	418.813[c]	1	1	
	8679.230	510.659	0.027(4)		
	11659.800	602.370	0.018(5)		
	11798.600	607.450	0.015(5)		
	12232.340	623.892	0.020(6)		
	12566.800	637.192	0.024(7)		
	13777.050	690.452	0.025(9)	0.010	
28445.430	838.220	362.121	1	1	
	1489.160	370.866	0.76(8)	0.547	
	2237.970	381.463	0.24(3)	0.247	
	2688.690	388.138	0.37(4)	0.265	

Table 2. (*continued*).

Upper level energy (cm^{-1})	Lower level energy (cm^{-1})	Transition wavelength (nm)	Relative intensity		
			This work	MCS[a]	XSQGB[b]
	3499.120	400.748	0.27(3)	0.276	
	4386.030	415.521[c]	0.64(7)	0.329	
	7524.860	477.865	w		
	8046.000	490.073	0.18(5)	0.024	
	8679.230	505.773	0.36(5)	0.038	
	11659.800	595.583	0.10(4)	0.015	
	15242.950	757.225		0.014	
28540.119	2237.970	380.089	0.41(5)	0.320	
	3052.650	392.239	1	1	
	3909.620	405.886	0.27(3)	0.176	
	4386.030	413.892	0.06(2)	0.020	
	5317.560	430.495[c]	0.23(3)	0.128	
	9406.630	522.499	0.024(5)		
	10214.380	545.529	0.020(7)		
	10960.160	568.672	0.06(1)	0.012	
	11791.050	596.883	0.05(1)	0.014	
	12045.100	606.079	w		
	12841.600	636.827	0.06(2)	0.009	
	13466.500	663.228	0.13(2)	0.016	
	13604.500	669.356	0.14(2)	0.028	
28725.529	1489.160	367.052	0.09(1)		
	2237.970	377.429	0.074(9)		
	3052.650	389.406	0.35(4)	0.494	
	3499.120	396.298	0.36(4)		
	4386.030	410.739	1	1[c]	
	5317.560	427.085[c]	0.48(5)	0.185	
	8679.230	498.707	w		
	9406.630	517.484	w		
	10960.160	562.737	w		
	11395.400	576.870	w		
	12789.810	627.348	w		
	13777.050	668.780	w	0.021	
28913.990	1489.160	364.529	0.29(3)	0.300	
	2237.970	374.762	0.27(3)	0.400	
	3052.650	386.568	0.040(5)	0.067	
	3499.120	393.359	0.19(2)		
	4386.030	407.583	0.64(6)	0.675	
	5317.560	423.674[c]	1	1	
	8679.230	494.062	0.041(5)		
	9406.630	512.484	0.064(8)	0.042	
	13777.050	660.453	0.08(1)	0.079	
28997.141	1489.160	363.427	1	1	
	2237.970	373.597	0.48(5)	0.471	
	3052.650	385.329	0.05(2)		
	5317.560	422.186[c]	0.028(6)		
	8046.000	477.168	w		
	8679.230	492.039	0.04(1)	0.022	

Table 2. (*concluded*).

Upper level energy (cm^{-1})	Lower level energy (cm^{-1})	Transition wavelength (nm)	Relative intensity		
			This work	MCS[a]	XSQGB[b]
	9406.630	510.309	0.15(4)	0.076	
	12045.170	589.739[d]	0.030(9)	0.013	
	12232.340	596.323[d]		0.007	
	12789.810	616.834	0.013(4)	0.004	
	15897.540	763.172		0.003	
29387.869	1489.160	358.337	0.32(6)	0.585	
	2237.970	368.221	0.11(3)		
	3499.120	386.159	0.09(3)		
	5317.560	415.333[c]	1	1	
	8679.230	482.756	0.032(7)		
	13777.050	640.404	0.07(2)	0.017	

[a]Refs. 6 and 7. The uncertainties are stated to be in the range of 15–25%.
[b]Ref. 14. The tabulated relative intensities have been derived from the calculated transition probabilities.
[c]Transition pumped by laser.
[d]Unresolved lines in this work.
[e]Blended line in Refs. 6 and 7.

Fig. 6. Histograms showing the level of agreement of our relative-intensity data with previous work. The abscissa is the difference between our measurement and a previous one, expressed in units of the standard deviation of that difference. (*a*) Comparison with refs. 6 and 7. (*b*) Comparison with ref. 14.

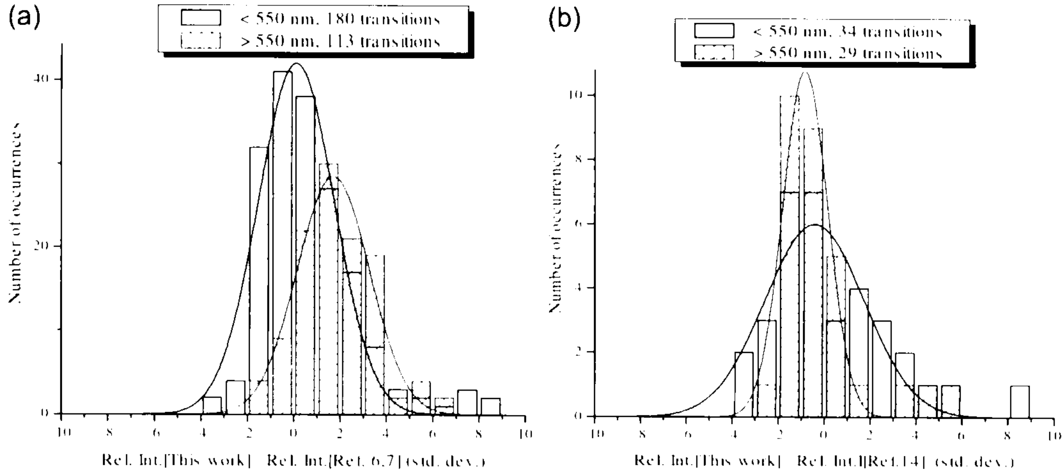

4. Results

The results of our relative intensity measurements for radiative transitions in Sm II are presented in Table 2. For each upper level, the intensity of the strongest branch that we observed is set to 1. Where possible, comparisons with the measurements of Meggers et al. [7] are presented, as well as with HFR calculations by Xu et al., [14] taken from the DREAM database [15]. An overall picture of the comparison is given in Fig. 6, which displays histograms of the differences between our results and those of Meggers et al. [6, 7] and Xu et al. [14]; these differences are in units of the standard deviation of the difference. Also included are best-fit Gaussian distributions. In Fig. 6*a* (Meggers et al.), we have somewhat arbitrarily used the upper limit of their stated 15–25% accuracy. The agreement is quite good for transitions with wavelengths $\lambda < 550$ nm, but there is a systematic shift for transitions with $\lambda > 550$ nm. Figure 6*b* (Xu et al.) shows better agreement in both wavelength ranges $\lambda < 550$ nm. The presence of a systematic shift for $\lambda > 550$ nm in only one of the comparisons suggests that the disagreement for this wavelength range is not due to a systematic error in our efficiency calibration. A number of interesting examples that exhibit the advantages of this new method can be drawn from Table 2. In the case of the 28 997.14 cm^{-1} level, the 385.33 nm transition to the 3 052.65 cm^{-1} level had never been experimentally observed before, and its relative intensity cannot be determined from measurements on a discharge lamp light source, because it is completely overlapped by a strong line in Sm I at 385.33 nm.

As another example, the transition at 396.301 nm was assigned by Meggers et al. [6, 7] to the upper energy level 25 552.801 cm^{-1}, and was the strongest branch from that level, with the lower level at 326.640 cm^{-1}. We saw no trace of this line in the spectrum for this upper level, but it appeared in our spectra as the strongest branch from the level at 27 464.199 cm^{-1}, and must have 2 237.970 cm^{-1} as its lower level. The difference in transition energy for these two assignments corresponds to a wavelength difference of only 0.001 nm. Nevertheless, highly selective laser excitation removes any ambiguity about the correct assignment. This assignment agrees with the predictions of Xu et al. [14].

Tables 3 and 4 present our BR measurements, along with spontaneous-emission transition probabilities $g_u A_{ul}$ and log $g_l f_{lu}$ values obtained by combining the BRs with our previously measured lifetime data [16]. Table 3 includes comparisons with the data of Xu et al. [14] and Corliss and Bozman [8] while Table 4 includes comparisons with the data of Saffman and Whaling [9]. Transitions are identified by the upper-level energy, angular momentum J and air wavelength, taken from the earlier references. When transitions not previously attributed to the upper level were observed, the air wavelengths were calculated from tabulated level energies [11, 12]. The transition probabilities and the oscillator strengths were calculated using the well-known formulas for electric dipole transitions

$$A_{ul} = \frac{R_{ul}}{\tau_u} \tag{3}$$

$$g_l f_{lu} = \frac{1}{0.66702\sigma_{ul}^2} g_u A_{ul} \tag{4}$$

where A_{ul} is the transition probability, R_{ul} is the branching ratio, τ_u is the upper-state lifetime, f_{lu} is the absorption oscillator strength, g_u and g_l are the $2J + 1$ statistical weights of the upper and lower levels, respectively, and σ_{ul} is the transition wave number (in cm^{-1}) [24].

5. Conclusions

We have measured 608 log ($g_l f_{lu}$) values for Sm II transitions over the wavelength range 358–876 nm. These transitions originate from 69 upper levels in the range 21 655–29 388 cm^{-1}. The log ($g_l f_{lu}$) values were obtained by combining measured relative intensities with previously measured radiative lifetimes. The uncertainties arose principally from systematics of the efficiency calibration of the optical detection system (7.1%), with smaller statistical contributions. Highly selective laser excitation of only a single upper level (usually a single hyperfine level) produces a simple fluorescence spectrum, removing any ambiguity in the assignment of transitions to a pair of energy levels.

Table 3. Transition probabilities and oscillator strengths derived from branching-ratio and lifetime data. Data from this work are compared with those of refs. 8 and 14. Branches that were observed but were too small to fit are indicated by the letter w. The issue of unobserved branches is discussed in the text.

					$g_u A_{ul}$ (10^6 s^{-1})			$\log(g_l f_{lu})$		
Upper level energy (cm^{-1})	J	Lifetime (ns)	Transition wavelength (nm)	Branching ratio	This work	XSQGB[a]	CB[b]	This work	XSQGB[a]	CB[b]
21655.420	0.5	51.9(5)	461.649	0.051(6)	2.0(2)		0.34	−2.20		−2.96
			468.719	0.69(2)	26.5(8)		6.6	−1.06		−1.66
			496.457	0.103(9)	4.0(4)		1.1	−1.83		−2.39
			508.707	0.054(5)	2.1(2)		0.75	−2.09		−2.53
			688.499	0.016(3)	0.6(1)			−2.36		
			764.507	0.09(1)	3.5(4)		2.0	−1.52		−1.76
			885.974							
21702.330	1.5	40.2(2)	460.651	0.21(2)	21(2)	26(8)	3.5	−1.18	−1.14	−1.96
			467.690	0.47(3)	46(3)	39(12)	12	−0.82	−0.94	−1.39
			479.158	0.11(1)	11(1)	4.4(2.2)	4.3	−1.43	−1.86	−1.83
			495.303	0.023(4)	2.3(4)		1.1	−2.08		−2.39
			525.792	w	w			w		
			686.281	0.05(2)	4.9(1.7)	6.8(3.4)	1.5	−1.46	−1.38	−1.96
			705.150	0.14(3)	14(3)	17(5)	3.7	−0.97	−0.96	−1.56
			923.190			2.2(1.1)			−1.64	
21904.119	1.5	70.8(6)	456.407	0.098(8)	5.5(5)		0.73	−1.76		−2.64
			463.316			6.2(3.1)			−1.75	
			474.568	0.6920(2)	39(1)	31(9)	9.1	−0.88	−1.04	−1.51
21904.119	1.5	70.8(6)	490.400	w	w			w		
			502.350	0.079(7)	4.5(4)		1.6	1.77		−2.22
			520.270	0.033(3)	1.9(2)		1.7	−2.12		−2.17
			695.255	0.013(2)	0.7(1)			−2.29		
			750.239	0.045(5)	2.5(3)		1.0	−1.67		−2.05
			800.156	0.042(8)	2.4(4)	2.8(1.4)	0.95	−1.64	−1.64	−2.04
			878.060			4.6(2.3)			−1.37	
			895.754			4.5(2.3)			−1.36	
			906.302			4.2(2.1)			−1.38	
22248.320	2.5	33.8(9)	456.042	0.107(8)	19(2)		3.2	−1.23		−2.00
			466.939	0.43(2)	77(4)		10	0.60		−1.48
			481.581	0.23(2)	41(3)		9.3	−0.85		−1.49
			493.809	0.058(5)	10.3(9)		3.5	−1.42		−1.90
			511.115	0.007(1)	1.3(2)			−2.30		
			533.208	0.004(1)	0.8(2)			2.47		
			661.488	0.006(1)	1.0(2)			−2.19		
			679.001	0.046(4)	8.2(7)		2.7	−1.24		1.73
			703.916	0.108(8)	19(2)		4.3	−0.85		−1.49
			878.878				1.3			−1.81
22875.410	3.5	39.9(1)	453.651	0.099(8)	20(2)	72(22)	4.3	1.21	−0.70	−1.88
			467.459	0.46(2)	93(4)	64(19)	27	0.52	−0.73	−1.05
			484.421	0.21(1)	41(3)	7.3(3.6)	8.1	−0.84	−1.64	−1.54
			495.237	0.079(6)	16(1)	4.7(2.4)	4.1	−1.23	1.80	−1.82
			515.951	0.010(1)	2.0(2)			−2.10		
			540.701	0.003(1)	0.5(1)			−2.66		
			651.263	0.004(1)	0.8(2)			−2.29		

Table 3. *(continued).*

Upper level energy (cm^{-1})	J	Lifetime (ns)	Transition wavelength (nm)	Branching ratio	$g_u A_{ul}$ ($10^6\ s^{-1}$) This work	XSQGB[a]	CB[b]	$\log(g_l f_{lu})$ This work	XSQGB[a]	CB[b]
			674.150	0.041(4)	8.2(7)	15(5)	2.8	−1.25	−1.05	−1.72
			704.221	0.095(7)	19(1)	28(8)	5.2	−0.85	−0.74	−1.42
			870.840			3.0(1.5)	3.2		−1.55	−1.44
			891.370			2.4(1.2)			−1.63	
23177.490	1.5	48.0(4)	431.332	0.032(3)	2.6(3)			−2.13		
			437.498	0.23(2)	19(1)	7.3(3.7)	5.5	−1.26	−1.73	−1.80
			447.517	0.076(7)	6.3(5)		1.3	−1.72		−2.42
			461.568	0.64(2)	53(2)	59(18)	8.4	−0.77	−0.78	−1.57
			472.139	w	w		0.81	w		−2.57
			487.936	w	w			w		
			638.694	0.011(5)	0.9(4)	7.0(3.5)		−2.25	−1.44	
			684.800	0.016(7)	1.3(6)			−2.04		
			812.508			1.4(7)	0.65		−1.95	−2.19
23260.949	3.5	53.8(6)	445.851	0.55(2)	82(3)		18	−0.61		−1.27
			459.181	0.18(1)	27(2)			−1.06		
			475.537	0.029(3)	4.3(4)		1.1	−1.84		−2.42
			485.956	0.064(5)	9.5(8)		2.6	−1.47		−2.04
			505.885	0.010(2)	1.5(2)			−2.24		
			657.067	0.046(4)	6.8(7)		3.4	−1.35		−1.66
			685.601	0.11(1)	17(2)		4.4	−0.92		−1.51
			891.356				7.8			−1.03
23646.900	4.5	42.5(1)	451.183	0.24(2)	56(4)		11	−0.77		−1.47
			466.964	0.41(2)	97(5)		13	−0.50		−1.38
			485.437	0.073(6)	17(1)		3.8	−1.22		−1.87
			496.194	0.098(8)	23(2)		7.7	−1.07		−1.54
			519.043	w	w			w		
			667.922	0.047(4)	11(1)		4.3	−1.13		−1.54
			702.040	0.14(1)	32(3)		6.4	−0.63		−1.33
			861.704				2.0			−1.66
			875.834				2.8			−1.48
23659.990	0.5	31.8(5)	422.535	0.15(2)	9.6(1.2)			−1.59		
			428.451	0.04(2)	2.3(1.1)			−2.20		
			451.510	0.74(3)	46(2)			−0.85		
			604.979	0.009(5)	0.5(3)			−2.52		
			662.890	0.038(9)	2.4(6)			−1.81		
			760.739	0.03(2)	1.7(1.0)			−1.83		
23842.199	2.5	33.6(3)	425.131	0.004(1)	0.8(2)			−2.68		
			434.585	0.19(1)	34(2)		11	−1.02		−1.49
			447.241	0.22(2)	39(3)		9.8	−0.94		−1.53
			457.769	0.424(2)	76(4)		13	−0.62		−1.40
			472.603	0.094(7)	17(1)		4.2	−1.25		−1.85
			491.430	0.015(2)	2.6(3)		0.47	−2.02		−2.77
			598.381	0.007(2)	1.2(4)			−2.18		
			612.676	w	w			w		
			632.889	0.009(3)	1.6(5)			−2.01		
			654.977	0.022(4)	3.9(7)		1.1	−1.61		−2.14

Table 3. (*continued*).

Upper level energy (cm^{-1})	J	Lifetime (ns)	Transition wavelength (nm)	Branching ratio	$g_u A_{ul}$ (10^6 s^{-1}) This work	$g_u A_{ul}$ (10^6 s^{-1}) XSQGB[a]	$g_u A_{ul}$ (10^6 s^{-1}) CB[b]	$\log(g_l f_{lu})$ This work	$\log(g_l f_{lu})$ XSQGB[a]	$\log(g_l f_{lu})$ CB[b]
			692.704	0.019(5)	3.3(9)		1.2	−1.62		−2.07
			787.998							
			803.199				1.4			−1.87
			820.631							
			830.088				0.91			−2.03
23962.250	1.5	22.54(6)	422.971	0.31(2)	56(3)		15	−0.82		−1.39
			432.329	0.26(2)	47(3)		12	−0.88		−1.46
			455.266	0.30(2)	54(3)		9.1	−0.78		−1.55
			469.936	0.065(5)	11.5(9)		4.0	−1.42		−1.88
			649.866	0.055(7)	9.7(1.2)		2.3	−1.21		−1.83
			756.287							
			763.793				1.9			−1.78
			821.896				2.3			−1.63
24013.561	1.5	69.1(2)	416.314	0.20(2)	11.5(9)			−1.52		
			422.055	0.048(6)	2.8(4)			−2.13		
			431.372	0.15(1)	8.7(7)			−1.62		
			454.205	0.60(2)	35(1)			−0.97		
24194.381	2.5	162.8(7)	428.032	0.23(2)	8.6(6)		1.9	−1.63		−2.27
			440.304	0.23(2)	8.6(6)		18	−1.60		−1.27
			450.504	0.43(2)	15.8(8)		4.1	−1.32		−1.90
			464.863	0.038(6)	1.4(2)			−2.35		
			483.068	0.023(6)	0.8(2)			2.54		
			586.027	0.04(1)	1.6(5)		0.89	−2.07		−2.34
24221.811	0.5	15.5(2)	418.377	0.30(2)	39(3)		12	−0.99		−1.52
			440.337	0.25(2)	32(2)		9.4	−1.03		−1.56
			449.948	0.41(2)	52(3)		8.6	−0.80		−1.58
			639.082	0.044(7)	5.7(9)		1.7	−1.46		−1.98
			721.807	w	w			w		
			758.833	w	w			w		
24257.369	4.5	46.6(3)	439.086	0.63(2)	135(4)	44(13)	37	−0.41	−0.91	−0.97
			454.018	0.088(8)	19(2)	89(27)	7.0	−1.23	0.58	−1.66
			471.461	0.052(5)	11(1)	14(4)	2.9	−1.43	1.34	−2.01
			481.602	0.058(6)	12(1)	7.5(3.8)	3.3	−1.37	−1.60	−1.93
			503.098	0.009(3)	1.9(7)			−2.13		
			641.748	0.041(5)	8.8(1.1)	15(5)	2.0	−1.26	−1.05	−1.91
			673.181	0.12(1)	25(3)	22(7)	8.8	−0.78	−0.84	−1.22
			710.200	0.010(2)	2.2(4)			−1.79		
			751.831	w	w			w		
			777.272	w	w			w		
			818.628	w	w	5.1(2.6)		w	−1.32	
			831.370	w	w	8.6(4.3)		w	−1.08	
			871.786	w	w	1.9(9)	3.4	w	−1.70	−1.42
			875.741	w	w	3.2(1.6)		w	−1.47	
24429.520	1.5	24.7(1)	409.225	0.34(2)	55(3)	62(19)	23	−0.86	−0.88	−1.23
			414.771	0.104(8)	17(1)		7.4	−1.36		−1.72
			423.766	0.24(2)	39(2)	8.4(4.2)	12	−0.98	−1.72	−1.50

Table 3. *(continued).*

Upper level energy (cm^{-1})	J	Lifetime (ns)	Transition wavelength (nm)	Branching ratio	$g_u A_{ul}$ (10^6 s^{-1}) This work	XSQGB[a]	CB[b]	$\log(g_l f_{lu})$ This work	XSQGB[a]	CB[b]
			436.345	0.115(8)	19(1)		5.3	−1.27		−1.82
			445.780	0.012(1)	1.9(2)			−2.24		
			459.835	0.071(6)	11.5(9)	7.5(3.8)	2.2	−1.44	−1.70	−2.15
			591.389	0.010(2)	1.6(3)			−2.06		
			630.708	0.034(3)	5.5(5)		2.6	−1.49		−1.82
			665.616	0.028(3)	4.6(5)	10(3)	2.2	−1.52	−1.27	−1.84
			711.143	0.005(1)	0.8(2)			−2.20		
			718.657			2.5(1.3)			−1.83	
			730.466	0.009(2)	1.4(3)			−1.95		
			737.466			7.3(3.6)			−1.35	
			753.133	0.006(2)	0.9(3)			−2.12		
			791.490	0.031(5)	5.0(8)		2.6	−1.33		−1.62
24582.590	2.5	19.6(3)	412.154	0.032(3)	9.7(9)		2.8	−1.61		−2.15
			421.034	0.14(1)	44(3)		16	−0.94		−1.37
			432.902	0.39(2)	119(6)		44	−0.47		−0.91
			442.758	0.063(5)	19(2)		4.5	−1.25		−1.88
			456.620	0.27(2)	83(5)		12	−0.59		−1.41
			474.173	0.021(2)	6.6(6)		2.0	−1.65		−2.17
			624.675	0.019(2)	5.7(5)		3.2	−1.48		−1.73
			658.902	0.008(1)	2.4(3)			−1.81		
			694.162	0.016(1)	4.8(5)		1.5	−1.46		−1.97
			710.835	0.003(1)	1.0(2)			−2.12		
			744.547	0.016(2)	4.9(6)			−1.39		
			773.614[c]		0.019(2)5.9(7)			−1.28		
			782.013[c]				1.7			−1.82
24588.000	5.5	40.7(5)	447.301	0.29(2)	85(5)	89(27)	16	−0.59	−0.62	−1.32
			464.223	0.42(2)	123(6)	103(10)	24	−0.40	−0.52	−1.12
			483.462	0.033(4)	9.8(1.2)	7.0(3.5)	3.3	−1.46	−1.65	−1.94
			494.863	0.12(1)	34(3)	8.2(4.1)	10	−0.90	−1.56	−1.43
			628.410							
			658.520	0.032(3)	9.3(1.0)	4.1(2.0)	3.4	−1.22	−1.64	−1.66
			695.527	0.113(9)	33(3)	41(12)	11	−0.62	−0.59	−1.11
			847.355			4.6(2.3)	2.2		−1.38	−1.63
			851.091			9.6(4.8)	3.6		−1.06	−1.41
			898.913			5.4(2.7)			−1.26	
			910.207			2.3(1.2)			−1.61	
24685.529	1.5	55.1(9)	404.981	0.30(2)	22(2)		14	−1.27		−1.46
			410.412	0.19(2)	14(1)		5.7	−1.46		−1.84
			419.216	0.22(2)	16(1)		4.0	−1.38		−1.97
			431.523	0.036(6)	2.6(4)			−2.13		
			440.749	0.08(1)	5.7(10)		1.5	−1.78		−2.35
			454.483	0.15(2)	11(1)		2.8	−1.48		−2.07
			569.627	0.029(9)	2.1(7)			−1.99		
			654.461				1.4			−2.04
24689.840	3.5	20.5(3)	430.901	0.18(1)	71(5)		23	−0.70		−1.20
			445.272	0.37(2)	143(8)		35	−0.37		−0.98

Table 3. (*continued*).

Upper level energy (cm^{-1})	J	Lifetime (ns)	Transition wavelength (nm)	Branching ratio	g_uA_{ul} (10^6 s^{-1}) This work	XSQGB[a]	CB[b]	$\log(g_lf_{lu})$ This work	XSQGB[a]	CB[b]
			454.394	0.30(2)	115(7)		22	−0.45		−1.17
			471.773	0.100(7)	39(3)		9.1	−0.88		−1.52
			492.381	0.013(1)	5.0(4)		2.6	−1.74		−2.03
			624.413	w	w		1.9	w		−1.95
			654.276	0.025(2)	9.8(8)			−1.20		
			728.149	0.017(2)	6.8(6)		2.5	−1.27		−1.69
			767.246							
			775.507				2.4			−1.67
			802.509				2.5			−1.63
			854.322				2.6			−1.54
24848.471	2.5	112(1)	407.685	0.126(9)	6.8(5)		2.2	−1.77		−2.25
			416.371	0.14(1)	7.3(5)		2.7	−1.72		−2.16
			427.974	0.42(2)	23(1)			−1.21		
			437.605	0.025(2)	1.3(1)			−2.42		
			468.267	0.17(1)	8.8(6)		3.4	−1.54		−1.95
			564.388	0.017(2)	0.9(1)			−2.36		
			577.087	0.016(2)	0.8(1)			−2.37		
			594.986	0.002(2)	0.1(1)			−3.19		
			614.467	0.011(2)	0.6(1)			−2.48		
			647.554	0.011(2)	0.6(1)			−2.43		
			697.646	0.005(3)	0.2(2)			−2.75		
			715.358	0.007(4)	0.4(2)			−2.57		
			730.090	0.022(5)	1.2(3)			−2.03		
			743.120	0.014(5)	0.8(3)			−2.20		
			758.018	0.022(7)	1.2(3)			−2.00		
24928.801	2.5	25.4(9)	406.354	0.32(2)	76(5)		14	−0.72		−1.45
			414.983	0.23(2)	54(4)		21	−0.85		−1.26
			426.508	0.16(1)	38(3)		14	−0.99		−1.43
			436.072	0.23(1)	53(4)		15	−0.82		−1.36
			449.512	0.012(2)	2.9(4)		0.67	−2.06		−2.69
			466.512	0.051(4)	12(1)		2.2	−1.40		−2.15
			611.448	w	w			w		
			677.866	w	w		3.8	w		−1.58
			761.393				1.3			−1.95
25055.539	1.5	34.9(5)	399.001	0.34(2)	39(3)		39	−1.03		−1.04
			404.271	0.38(3)	44(3)		20	−0.97		−1.32
			412.811	0.022(3)	2.6(4)			−2.18		
			424.739	0.038(4)	4.4(5)		1.4	−1.92		−2.41
			433.674	0.046(5)	5.3(6)			−1.83		
			446.965	0.079(7)	9.1(9)			−1.57		
			638.983	0.05(1)	5.6(1.1)		2.5	−1.47		−1.82
			687.708							
			704.913	0.04(4)	4.4(4.1)			−1.48		
25175.320	2.5	81(3)	402.322	0.63(2)	47(2)		24	−0.94		−1.23
			410.779	0.046(5)	3.4(4)		1.6	−2.06		−2.38
			422.069	0.027(4)	2.0(3)			−2.27		

Table 3. (*continued*).

Upper level energy (cm^{-1})	J	Lifetime (ns)	Transition wavelength (nm)	Branching ratio	$g_u A_{ul}$ ($10^6\ s^{-1}$) This work	XSQGB[a]	CB[b]	$\log(g_l f_{lu})$ This work	XSQGB[a]	CB[b]
			431.433	0.028(4)	2.1(3)			−2.23		
			444.584	0.054(6)	4.0(5)			−1.92		
			461.207	0.018(4)	1.4(3)			−2.36		
			554.162	w	w			w		
			583.633	0.09(1)	6.4(9)		3.5	−1.48		−1.75
			666.722	0.11(2)	7.9(1.6)		1.7	−1.28		−1.95
25178.449	1.5	23.5(2)	397.053	0.25(2)	42(3)		20	−1.01		−1.33
			402.272	0.027(3)	4.6(5)		2.4	−1.95		−2.23
			410.727	0.103(8)	18(1)		23	−1.35		−1.24
			422.532	0.60(2)	101(4)		30	−0.57		−1.10
			431.374	0.029(3)	4.9(6)		5.2	−1.86		−1.84
25304.090	3.5	22.2(6)	419.786	0.007(1)	2.6(3)		1.3	−2.17		−2.46
			433.414	0.20(2)	72(7)		40	−0.69		−0.94
			442.052	0.23(2)	81(7)		46	−0.62		−0.87
			458.483	0.12(1)	44(4)		18	−0.85		−1.24
			477.923	0.004(1)	1.4(2)			−2.31		
			579.278	w	w			w		
			601.343	w	w			w		
			628.991	0.007(1)	2.7(5)		2.3	−1.80		−1.87
			732.706	0.43(3)	156(12)			0.10		
			764.798				2.4			−1.68
			811.714				1.2			−1.93
25361.449	1.5	16.8(2)	394.188	0.27(2)	63(4)		35	−0.83		−1.08
			399.331	0.23(2)	55(4)		21	−0.88		−1.30
			407.662	0.083(6)	20(2)		8.2	−1.31		−1.69
			427.994	0.16(1)	39(3)		7.2	−0.97		−1.70
			440.934	0.20(1)	48(3)		16	−0.85		−1.32
			626.729	0.054(6)	13(1)		9.3	−1.12		−1.26
			673.535	w	w			w		
			690.029				1.0			−2.14
			698.417	w	w			w		
25385.359	5.5	42.2(2)	431.893	0.69(2)	195(6)	182(18)	60	−0.26	−0.32	−0.78
			447.648							
			465.511	0.08(1)	24(3)	7.5(3.8)	4.9	−1.11	−1.64	−1.79
			476.073	0.011(3)	3.1(10)			−1.98		
			498.172	0.007(4)	2.0(1.0)		3.2	−2.12		−1.93
			625.659	0.025(3)	7.2(8)	4.8(2.4)	4.0	−1.37	−1.59	−1.63
			658.971	0.086(8)	24(2)	21(6)	11	−0.80	−0.91	−1.14
			693.040	0.015(2)	4.4(6)	6.6(3.3)	1.8	−1.50	−1.36	−1.88
			735.399	0.004(2)	1.1(5)			−2.06		
			749.408	0.008(2)	2.3(6)			−1.71		
			793.713[c]	0.015(4)	4.2(1.0)		2.5	−1.40		−1.62
			796.990[c]							
			838.776	0.018(7)	5.2(1.9)	13(4)	2.7	−1.26	−0.91	−1.55
			848.601	0.04(1)	12(3)	25(8)	6.3	−0.89	−0.61	−1.17

Table 3. (*continued*).

Upper level energy (cm^{-1})	J	Lifetime (ns)	Transition wavelength (nm)	Branching ratio	$g_u A_{ul}$ (10^6 s^{-1}) This work	XSQGB[a]	CB[b]	$\log(g_l f_{lu})$ This work	XSQGB[a]	CB[b]
25417.141	2.5		398.445	0.037(4)						
			406.738	0.20(1)						
			417.803	0.49(2)						
			426.976	0.12(1)			1.1			−2.50
			439.854	0.014(5)						
			456.118	0.14(1)			0.59			−2.74
			558.746	w						
			593.715	w						
			624.549	w						
			671.017	w						
			700.979	w						
			712.982	w						
			726.685	w						
			734.091	w						
25552.801	1.5	79(1)	396.302							
			404.505	0.46(2)	23(1)		17	−1.25		−1.38
			415.951	0.17(1)	8.7(6)		3.2	−1.65		−2.08
			424.517	0.34(2)	17(1)		3.8	−1.33		−1.99
			437.244	0.029(3)	1.5(1)			−2.38		
			588.970	w	w			w		
			619.300	w	w			w		
			675.061	w	w			w		
			689.204	w	w			w		
25565.971	3.5	31.1(5)	404.290	0.32(2)	83(5)		27	−0.69		−1.18
			415.220	0.30(2)	78(5)		37	−0.69		−1.02
			428.549	0.21(1)	54(4)		1.7	−0.83		−2.34
			436.992	0.067(6)	17(1)		6.8	−1.31		−1.71
			472.013	0.031(3)	7.9(9)		1.8	−1.58		−2.21
			618.795	w	w		2.1	w		−1.92
			649.793	0.020(8)	5.0(2.0)			−1.50		
			684.470	0.05(1)	13(3)		6.1	−1.06		−1.37
			705.493	w	w		2.0	w		−1.83
			726.155							
			739.398							
			794.813				2.2			−1.68
25597.699	4.5	14.2(1)	414.674	0.019(3)	14(2)		5.1	−1.46		−1.88
			427.967	0.18(1)	126(9)		39	−0.46		−0.97
			443.432	0.46(2)	324(15)		60	−0.02		−0.75
			452.391	0.21(2)	147(10)		22	−0.35		−1.16
			471.307	0.073(7)	51(5)		15	−0.77		−1.30
			492.956	0.012(4)	8.3(3.0)		1.7	−1.52		−2.22
			648.455	0.018(3)	13(2)		3.7	−1.09		−1.64
			682.986	0.012(4)	8.5(2.6)		3.1	−1.22		−1.67
			703.918	w	w			w		
			724.089	0.017(7)	12(5)		7.3	−1.03		−1.24
			737.666				3.3			−1.57

Table 3. (*continued*).

Upper level energy (cm^{-1})	J	Lifetime (ns)	Transition wavelength (nm)	Branching ratio	$g_u A_{ul}$ (10^6 s^{-1}) This work	XSQGB[a]	CB[b]	$\log(g_l f_{lu})$ This work	XSQGB[a]	CB[b]
			783.723				3.5			−1.49
			792.813				13			−0.93
			824.094				2.3			−1.63
			870.636				2.0			−1.65
25664.971	6.5	44.4(2)	442.113	0.38(2)	119(6)		33	−0.46		−1.01
			459.528	0.33(2)	105(6)			−0.48		
			491.326	0.113(9)	36(3)		20	−0.89		−1.13
			614.899	0.003(1)	0.9(4)			−2.30		
			647.046	0.024(3)	7.4(8)		1.9	−1.33		−1.93
			686.110	0.122(9)	38(3)			−0.57		
			720.578	0.003(2)	1.0(7)			−2.09		
			819.550	0.024(7)	7.6(2.2)		2.8	−1.11		−1.55
			828.927	w	w		2.9	w		−1.53
			863.289	w	w		3.5	w		−1.41
25790.150	3.5	57.3(3)	400.657	0.098(7)	14(1)		6.2	−1.48		−1.83
			411.390	0.24(2)	34(2)		14	−1.07		−1.46
			424.470	0.42(2)	58(3)		21	−0.80		−1.24
			432.751	0.047(4)	6.6(5)		1.5	−1.74		−2.36
			448.486	0.010(1)	1.4(1)			−2.39		
			467.069	0.056(4)	7.9(6)			−1.59		
			547.335	0.014(2)	2.0(2)			−2.05		
			584.260	0.025(3)	3.5(4)		2.1	−1.75		−1.97
			610.326	0.026(3)	3.6(4)			−1.69		
			640.461	0.010(3)	1.4(4)			−2.08		
			674.124	0.056(6)	7.9(8)			−1.27		
25939.869	6.5	62.4(3)	436.802	0.20(1)	44(3)		18	−0.90		−1.28
			453.794	0.51(2)	114(5)		27	−0.45		−1.08
			484.776	0.18(1)	40(3)		8.4	−0.85		−1.53
			635.735	0.016(5)	3.6(1.0)			−1.66		
			673.405	0.10(1)	23(2)		8.4	−0.81		−1.25
			801.488				3.0			−1.54
			843.271				5.2			−1.25
25980.320	2.5	19.9(4)	389.697	0.31(2)	93(6)		59	−0.68		−0.87
			397.627	0.17(1)	51(4)		32	−0.92		−1.11
			408.195	0.024(2)	7.3(7)		4.6	−1.74		−1.94
			416.947	0.21(1)	64(4)		29	−0.77		−1.12
			429.218	0.14(1)	42(3)		13	−0.94		−1.45
			444.691	0.017(2)	5.0(5)		1.7	−1.82		−2.30
			603.322	0.010(2)	3.0(5)		1.9	−1.79		−1.99
			632.752	0.046(4)	14(1)		7.9	−1.08		−1.32
			661.761	0.006(2)	1.7(6)			−1.96		
			669.472	0.008(2)	2.4(6)			−1.79		
			685.451	0.012(3)	3.5(8)		1.7	−1.60		−1.92
			745.311	0.05(1)	14(3)		3.7	−0.92		−1.51

Table 3. (*continued*).

Upper level energy (cm^{-1})	J	Lifetime (ns)	Transition wavelength (nm)	Branching ratio	$g_u A_{ul}$ (10^6 s^{-1})			$\log(g_l f_{lu})$		
					This work	XSQGB[a]	CB[b]	This work	XSQGB[a]	CB[b]
26046.350	4.5	20.9(8)	434.780	0.29(2)	141(10)		42	−0.40		−0.93
			443.389	0.50(2)	237(14)		62	−0.15		−0.74
			461.544	0.14(1)	67(6)		12	−0.67		−1.42
			482.286	0.0035(5)	1.7(2)			−2.23		
			555.391	0.0020(3)	1.0(2)			−2.35		
			575.641	0.0024(4)	1.2(2)			−2.24		
			600.806	0.0042(5)	2.0(2)			−1.97		
			630.118	0.010(1)	4.6(5)		2.4	−1.56		−1.84
			723.703	0.014(1)	6.6(7)		1.9	−1.29		−1.84
			754.137[c]	0.025(2)			3.4			−1.54
			757.095[c]				3.4			−1.54
			765.575	0.009(1)	4.5(6)		1.6	−1.41		−1.86
26086.631	3.5	70(2)	395.953	0.22(2)	25(2)			−1.23		
			406.431	0.20(1)	22(2)			−1.26		
			419.193	0.32(2)	36(2)			−1.02		
			442.598	0.050(5)	5.7(5)			−1.78		
			460.688	0.086(7)	9.8(9)			−1.51		
			574.309	0.009(5)	1.0(5)			−2.30		
			628.523	0.013(7)	1.5(8)			−2.06		
			692.962	0.03(1)	3.5(1.6)			1.60		
			711.980	0.08(2)	9.2(2.4)			−1.15		
26159.600	3.5	93(4)	394.811	0.79(3)	68(4)		26	−0.80		−1.21
			405.229	0.022(5)	1.9(4)			−2.34		
			425.939	0.037(5)	3.2(5)		2.0	−2.06		−2.27
			441.173	0.034(5)	2.9(5)			−2.07		
			459.144	0.011(4)	0.9(4)			−2.54		
			551.918	0.010(7)	0.9(6)			−2.41		
			571.912	0.028(9)	2.4(8)			−1.92		
			689.475	0.07(3)	5.8(2.8)			−1.38		
26190.920	2.5	39.3(3)	386.524	0.110(8)	17(1)		12	−1.42		1.56
			394.324	0.29(2)	44(3)		22	0.99		−1.29
			404.715	0.33(2)	50(3)		27	0.91		−1.18
			413.317	0.045(4)	6.8(6)		3.9	−1.76		−2.01
			425.372	0.036(3)	5.6(5)			−1.82		
			440.564	0.033(3)	5.1(5)		1.5	−1.83		−2.37
			595.750	0.027(5)	4.2(7)		2.4	1.65		−1.90
			624.429	0.039(6)	6.0(10)			1.46		
			652.663	0.031(8)	4.7(1.2)			−1.52		
			664.904	w	w			w		
			694.624	0.06(1)	9.7(1.9)			−1.15		
26214.051	2.5	66(1)	386.179	0.14(1)	12.5(9)			−1.55		
			393.964	0.038(3)	3.5(3)		1.8	−2.09		−2.37
			404.337	0.057(5)	5.2(4)			−1.90		
			412.922	0.32(2)	29(2)		11	−1.13		−1.57
			424.954	0.28(2)	26(2)		8.0	1.16		−1.67
			440.116	0.16(1)	15(1)			−1.36		

Table 3. (*continued*).

Upper level energy (cm^{-1})	J	Lifetime (ns)	Transition wavelength (nm)	Branching ratio	$g_u A_{ul}$ (10^6 s^{-1}) This work	$g_u A_{ul}$ XSQGB[a]	$g_u A_{ul}$ CB[b]	$\log(g_l f_{lu})$ This work	$\log(g_l f_{lu})$ XSQGB[a]	$\log(g_l f_{lu})$ CB[b]
26357.900	2.5	32.2(3)	384.045	0.18(1)	33(3)	80(24)	16	−1.14	−0.78	−1.45
			391.744	0.22(2)	41(3)		23	−1.02		−1.28
			401.998	0.13(1)	24(2)	17(5)	11	−1.23	−1.40	−1.59
			410.483	w	w			w		
			422.371	0.12(1)	22(2)	23(7)	5.9	−1.23	−1.24	−1.80
			437.346	0.29(2)	54(4)		18	−0.81		−1.28
			589.880	w	w			w		
			617.983	0.030(6)	5.6(1.1)	9.0(4.5)	2.6	−1.50	−1.32	−1.83
			631.163							
			645.625							
			657.601							
			668.153	0.038(9)	7.1(1.7)	9.3(4.6)	2.3	−1.33	−1.25	−1.81
			855.201			2.3(1.1)			−1.62	
26505.529	5.5	12.7(3)	411.957	0.018(2)	17(2)		6.0	−1.35		−1.82
			426.267	0.13(1)	120(10)		53	−0.49		−0.84
			442.434	0.54(2)	512(23)		130	0.18		−0.42
			451.963	0.16(1)	154(12)		40	−0.33		−0.92
			471.834	0.049(4)	46(4)		14	−0.81		−1.34
			643.101	0.008(1)	7.7(1.2)		2.8	−1.32		−1.76
			679.415	0.037(3)	35(3)		14	−0.61		−1.02
			728.890	w	w		2.7	w		−1.67
			731.653	0.004(2)	3.6(1.5)			−1.54		
			766.717	w	w		3.4	w		−1.53
			774.919	0.009(3)	8.4(2.6)		5.6	−1.12		−1.29
			804.868'	0.043(6)			7.0			−1.17
			806.846'				8.2			−1.10
26540.119	6.5	34.0(4)	425.639	0.66(2)	271(8)		88	−0.13		−0.62
			441.758	0.111(9)	46(4)		17	−0.88		−1.31
			471.065	0.033(3)	13(1)		4.2	−1.35		−1.86
			612.360	0.013(1)	5.4(5)		2.7	−1.52		−1.82
			647.235	0.063(5)	26(2)		5.7	−0.79		−1.45
			677.822	0.021(2)	8.7(8)		3.0	−1.22		−1.69
			727.056	0.005(1)	2.0(3)			−1.80		
			772.847	0.017(2)	7.0(7)		5.7	−1.20		−1.29
			802.633	0.023(2)	9.6(1.0)		4.1	−1.03		−1.40
			830.582	0.057(6)	23(2)		7.3	−0.62		−1.12
26565.609	4.5	65.6(4)	398.668	0.34(2)	52(3)		30	−0.91		−1.15
			410.939	0.20(1)	31(2)		17	−1.10		−1.36
			425.178	0.16(1)	25(2)		11	−1.17		−1.54
			433.408	0.018(2)	2.8(3)			−2.10		
			450.739	0.011(2)	1.6(2)			−2.30		
			470.500	0.013(2)	2.0(3)			−2.18		
			539.819	0.019(3)	2.8(4)			−1.90		
			558.930	0.011(3)	1.7(4)			−2.09		
			640.625	0.057(7)	8.8(1.1)		1.5	−1.27		−2.03

Table 3. (*continued*).

Upper level energy (cm^{-1})	J	Lifetime (ns)	Transition wavelength (nm)	Branching ratio	$g_u A_{ul}$ (10^6 s^{-1}) This work	XSQGB[a]	CB[b]	$\log(g_l f_{lu})$ This work	XSQGB[a]	CB[b]
			659.005	w	w			w		
			676.652	0.039(8)	5.9(1.3)		2.0	−1.39		−1.86
			688.495	0.034(9)	5.2(1.4)			−1.44		
			697.485	0.03(1)	4.2(1.5)			−1.51		
			725.711	0.06(2)	9.7(2.5)		1.5	−1.12		−1.92
26599.080	1.5	17.9(2)	375.846	0.12(1)	27(3)		19	−1.24		−1.39
			388.076	0.21(2)	48(4)		35	−0.97		−1.10
			398.599	0.053(6)	12(1)		6.0	−1.55		−1.85
			406.458	0.19(2)	42(3)			−0.98		
			418.110	0.18(1)	40(3)		23	−0.98		−1.23
			513.626	0.017(6)	3.9(1.4)			−1.82		
			621.696	0.03(2)	7.3(3.3)			−1.37		
			630.514	0.04(2)	8.0(3.6)			−1.32		
			635.723	0.06(2)	12(4)			−1.13		
			642.836	0.08(2)	17(4)			−0.97		
			675.467	0.03(3)	7.2(5.8)		2.5	−1.31		−1.76
26723.869	1.5	47(1)	378.720	0.16(1)	13(1)		14	−1.55		−1.52
			386.205	0.45(2)	38(2)		30	−1.07		−1.17
			404.406	0.22(2)	18(1)			−1.35		
			415.940	0.18(1)	15(1)		4.5	−1.40		−1.93
26820.811	4.5	35.2(3)	394.651	0.19(1)	55(4)		21	−0.89		−1.30
			406.673	0.28(2)	80(5)		36	−0.70		−1.05
			420.612	0.28(2)	79(5)		30	−0.68		−1.10
			428.665	0.14(1)	39(3)		16	−0.97		−1.35
			445.611	0.039(3)	11.1(9)		4.3	−1.48		−1.90
			464.916	0.011(2)	3.2(5)			−1.99		
			574.086	0.013(3)	3.7(8)			−1.74		
			600.792	0.015(3)	4.2(10)			−1.65		
			630.317	0.032(5)	9.1(1.4)			−1.27		
			665.163	w	w		3.2	w		−1.68
			712.511	w	w		4.0	w		−1.52
26828.289	5.5	27.3(4)	420.480	0.005(1)	2.0(3)	40(12)	2.3	−2.28	−1.03	−2.21
			436.203	0.11(1)	49(4)	11(3)	38	−0.85	−1.54	−0.96
			445.463	0.21(2)	94(8)	290(29)	57	−0.55	−0.11	−0.77
			464.754	0.034(3)	15(1)		4.4	−1.32		−1.84
			573.839			3.1(1.5)			−1.88	
			601.739			8.0(4.0)	2.4		−1.43	−1.88
			664.832			4.0(2.0)			−1.65	
			712.132			2.6(1.3)			−1.78	
			748.197	0.24(3)	104(11)		4.8	−0.06		−1.40
			756.005	0.09(2)	41(7)	5.0(2.5)	2.2	−0.46	−1.45	−1.73
			784.483[c]	0.31(4)			2.0			−1.73
			786.362[c]			1.1(5)	3.8		−2.02	−1.46
			914.599			1.5(8)			−1.78	
			978.896			24(7)			−0.52	

Table 3. (*continued*).

Upper level energy (cm^{-1})	J	Lifetime (ns)	Transition wavelength (nm)	Branching ratio	$g_u A_{ul}$ (10^6 s^{-1}) This work	XSQGB[a]	CB[b]	$\log(g_l f_{lu})$ This work	XSQGB[a]	CB[b]
26880.600	5.5	48.4(6)	419.557	0.008(1)	2.1(2)			−2.26		
			435.210	0.35(2)	87(5)			−0.61		
			444.427	0.45(2)	112(6)			−0.48		
			463.627	0.087(7)	22(2)			−1.16		
			549.257	0.007(1)	1.7(3)			−2.12		
			572.122	0.011(1)	2.6(3)			−1.89		
			627.950	0.009(1)	2.3(3)			−1.86		
			662.527	0.009(2)	2.3(4)			−1.82		
			673.876	0.002(1)	0.6(2)			−2.41		
			712.105	0.009(2)	2.3(4)			−1.76		
			745.279	0.020(3)	4.9(7)			−1.39		
			781.276							
			783.140	0.034(5)	8.4(1.1)			−1.11		
26974.670	2.5	54.4(7)	375.156	0.095(7)	10.5(8)		7.5	−1.66		−1.80
			382.499	0.087(7)	9.6(8)			−1.68		
			392.269	0.082(7)	9.1(7)	7.5(3.8)	3.9	−1.68	−1.79	−2.04
			400.344	0.24(2)	27(2)	57(17)	13	−1.19	−0.90	−1.52
			411.644	0.21(1)	23(2)	21(6)	8.9	−1.24	−1.30	−1.65
			425.855	0.29(2)	32(2)	9.3(4.7)	9.9	−1.06	−1.63	−1.57
			528.152	w	w	3.2(1.6)		w	−1.92	
			543.447	w	w			w		
			658.750	w	w	0.2(1)		w	−1.85	
			812.342			1.4(7)			−1.88	
27107.619	3.5	41.4(2)	380.563	0.13(1)	25(2)		16	−1.26		−1.47
			390.233	0.025(5)	4.9(9)		3.4	−1.95		−2.11
			401.983	0.070(7)	14(1)		5.6	−1.48		−1.87
			409.403	0.16(1)	31(2)		14	−1.11		−1.45
			423.457	0.49(2)	94(4)		31	−0.60		−1.08
			439.987	0.060(7)	12(1)		4.6	−1.47		−1.88
			542.491	0.012(3)	2.4(6)			−1.97		
			619.122	0.018(6)	3.4(1.1)			−1.71		
			663.721	0.04(1)	6.8(1.9)			−1.35		
			687.529	w	w		1.7	w		−1.93
27165.350	2.5	64(3)	372.490	0.30(2)	28(2)	20(6)	21	−1.24	−1.45	−1.36
			379.729	0.20(2)	19(2)		21	−1.38		−1.34
			389.356							
			397.310	0.049(7)	4.6(7)			−1.96		
			408.437	0.21(2)	20(2)	9.1(4.6)	11	−1.31	−1.70	−1.57
			422.424	0.075(8)	7.1(8)		2.6	−1.72		−2.16
			509.010	0.048(7)	4.5(7)			−1.75		
			522.885	0.10(1)	9.3(1.1)			−1.42		
			537.871	0.017(6)	1.6(5)			−2.15		
			799.947			1.5(8)			−1.92	

Table 3. (*continued*).

Upper level energy (cm^{-1})	J	Lifetime (ns)	Transition wavelength (nm)	Branching ratio	$g_u A_{ul}$ (10^6 s^{-1})			$\log(g_l f_{lu})$		
					This work	XSQGB[a]	CB[b]	This work	XSQGB[a]	CB[b]
27188.301	3.5	26.9(4)	379.398	0.32(8)	95(23)		80	−0.69		−0.76
			389.008	0.16(5)	46(15)		32	−0.98		−1.14
			400.683	0.02(1)	7.1(3.0)		4.2	−1.77		−1.99
			408.055	0.09(3)	25(9)		12	−1.20		−1.54
			422.015	0.08(3)	23(8)		8.9	−1.20		−1.62
			438.430	0.10(4)	30(11)		15	−1.06		−1.35
			540.126	0.010(6)	3.0(1.7)			−1.89		
			587.810	0.02(1)	5.9(3.3)		1.9	−1.52		−2.01
			616.043	0.04(3)	12(8)		3.3	−1.17		−1.73
			633.021	0.02(2)	7.1(5.6)			−1.37		
			660.183	0.10(5)	30(13)		7.0	−0.71		−1.34
			668.445	0.04(3)	12(9)			−1.08		
27263.250	7.5	29.2(2)	428.079	0.80(2)	437(9)		120	0.08		−0.50
			618.289	0.015(1)	8.2(8)		4.5	1.33		−1.59
			656.929	0.15(1)	81(7)		24	−0.28		−0.81
			758.591	0.010(1)	5.5(6)		6.8	−1.32		−1.23
			783.509	0.029(3)	16(2)		8.5	−0.83		−1.11
27284.689	2.5	17.3(2)	370.841	0.14(1)	48(4)	35(10)	24	−1.01	−1.19	−1.30
			378.015	0.013(2)	4.5(5)			−2.01		
			387.554	0.14(1)	47(3)		30	−0.98		−1.18
			406.455	0.24(2)	84(5)	145(15)	70	−0.68	−0.49	−0.76
			420.305	0.32(2)	113(6)	104(10)	57	−0.53	−0.61	−0.82
			519.642	0.006(2)	2.1(5)	2.9(1.4)		−2.07	−1.99	
			615.692	0.016(3)	5.5(1.2)	3.6(1.8)		−1.50	−1.72	
			619.815	0.021(4)	7.2(1.3)			1.38		
			629.181	0.031(4)	11(1)	2.4(1.2)	8.0	−1.20	−1.92	−1.32
			639.828	0.021(4)	7.3(1.5)			−1.35		
			645.562	0.028(5)	9.6(1.6)	12(4)	2.3	−1.22	−1.15	−1.83
			679.258	0.027(6)	9.4(2.1)		2.5	−1.19		−1.77
			699.263			2.2(1.1)			−1.80	
			792.380			2.0(1.0)			−1.78	
			892.059			1.3(6)			−1.87	
			972.534			3.4(1.7)			−1.36	
27309.730	4.5	38(2)	387.178	0.23(2)	61(5)		42	−0.87		−1.02
			398.742	0.113(9)	30(3)		18	−1.15		−1.36
			412.135	0.18(1)	46(4)		21	−0.93		−1.27
			436.107	0.13(1)	34(3)		12	1.01		−1.47
			454.580	0.030(3)	7.9(9)		1.7	1.61		−2.29
			583.643	0.037(8)	9.6(2.1)			−1.31		
			611.468	0.05(1)	14(3)		2.8	1.11		−1.81
			663.062	0.04(1)	11(4)		2.4	1.12		−1.80
			688.519	0.19(2)			5.0			−1.45
			690.984				2.5			−1.74

Table 3. (*continued*).

Upper level energy (cm^{-1})	J	Lifetime (ns)	Transition wavelength (nm)	Branching ratio	$g_u A_{ul}$ (10^6 s^{-1}) This work	XSQGB[a]	CB[b]	log($g_l f_{lu}$) This work	XSQGB[a]	CB[b]
27464.199	3.5	36.9(8)	375.466	0.017(2)	3.8(5)			−2.10		
			384.876	0.056(5)	12(1)	27(8)		−1.57	−1.24	
			396.301	0.33(2)	70(4)			−0.78		
			403.510	0.31(2)	67(4)	26(8)	39	−0.79	−1.21	−1.03
			417.156	0.19(1)	41(3)	8.6(4.3)	22	−0.97	−1.66	−1.24
			433.189	0.010(1)	2.1(3)			−2.22		
			532.193	0.010(2)	2.2(4)			−2.04		
			553.734	0.006(2)	1.4(4)			−2.21		
			578.426			6.7(3.3)			−1.49	
			602.573			4.5(2.2)			−1.63	
			605.745			5.3(2.7)			−1.55	
			622.152			6.1(3.0)			−1.47	
			632.560	0.035(5)	7.5(1.1)	0.5(2)		−1.35	−1.58	
			648.370	0.016(4)	3.5(9)	12(4)		−1.66	−1.15	
			656.337	0.029(5)	6.3(1.2)	3.3(1.7)		−1.39	−1.69	
			671.073	w	w			w		
			818.022			1.7(8)			−1.76	
27695.961	6.5	24.6(5)	420.291	0.067(6)	38(4)	67(20)	38	−1.00	−0.80	−1.00
			446.734	0.902(9)	513(12)	592(59)	140	0.19	0.19	−0.39
			602.174	0.006(2)	3.4(9)			−1.73		
			628.563							
			702.574							
			734.475							
			757.810	0.025(4)	14(3)	17(5)	4.6	−0.90	−0.94	−1.40
			902.242			1.8(9)			−1.73	
			970.224			46(14)			−0.28	
28072.330	3.5	9.96(9)	367.082	0.31(2)	248(14)		150	−0.30		−0.52
			376.071	0.20(1)	163(11)		120	−0.46		−0.60
			393.843	w	w		1.8	w		−2.38
			406.832	0.107(8)	86(6)		44	−0.67		−0.96
			422.066	0.22(1)	176(11)		48	−0.33		−0.89
			486.539							
			499.203	0.037(4)	30(3)		11	−0.95		−1.37
			515.504	0.104(9)	83(7)		58	−0.48		−0.63
			581.266							
			599.465	0.022(6)	18(5)		4.8	−1.02		−1.59
			623.766				5.7			−1.48
			644.753							
			699.340							
28151.400	5.5	29.3(4)	385.791	0.10(1)	42(4)		32	−1.03		−1.14
			398.314	0.24(2)	97(7)		46	−0.64		−0.96
			412.395	0.20(2)	82(6)		46	−0.68		−0.93
			420.662	0.14(1)	59(5)		18	−0.81		−1.33
			437.824	0.23(2)	93(7)		61	−0.57		−0.76
			611.065	0.044(6)	18(2)		8.5	−1.00		−1.32
			687.242	0.05(1)	18(4)		6.4	−0.89		−1.35
			712.237	w	w		3.0	w		−1.65

Table 3. (*continued*).

Upper level energy (cm^{-1})	J	Lifetime (ns)	Transition wavelength (nm)	Branching ratio	$g_u A_{ul}$ (10^6 s^{-1}) This work	XSQGB[a]	CB[b]	$\log(g_l f_{lu})$ This work	XSQGB[a]	CB[b]
28191.961	4.5	37(1)	374.387	0.38(2)	104(7)			−0.66		
			385.188	0.15(2)	41(4)		29	−1.04		−1.19
			404.861	0.047(9)	13(2)		13	−1.51		−1.49
			419.945	0.16(2)	44(4)		18	−0.94		−1.33
			437.047	0.06(1)	16(3)		3.1	−1.33		−2.06
			512.344	w	w			w		
			532.183	0.033(7)	9.0(2.0)			−1.42		
			555.054	0.022(7)	5.9(2.0)			−1.56		
			580.162	w	w		1.6	w		−2.08
			619.147	w	w			w		
			626.408	w	w			w		
			649.081	0.14(2)	38(5)		6.1	−0.62		−1.42
28256.320	3.5	35.7(2)	364.619	0.006(1)	1.3(2)			−2.57		
			373.486	0.023(2)	5.1(5)			−1.97		
			384.235	0.089(7)	20(2)		18	−1.36		−1.39
			391.009	0.038(4)	8.6(10)		5.6	−1.71		−1.89
			403.809	0.071(7)	16(1)		9.6	−1.41		−1.63
			418.813	0.65(2)	146(5)		70	−0.42		−0.74
			510.659	0.021(3)	4.7(6)			−1.73		
			602.370	0.017(5)	3.8(1.1)			−1.69		
			607.450	0.014(5)	3.1(1.0)			−1.76		
			623.892	0.019(6)	4.4(1.3)			−1.59		
			637.192	0.024(7)	5.3(1.5)			−1.49		
			690.452	0.027(9)	6.0(2.1)			−1.37		
28445.430	3.5	12.5(2)	362.121	0.23(2)	147(10)		130	−0.54		−0.60
			370.866	0.18(1)	114(8)		65	−0.63		−0.87
			381.463	0.058(5)	37(3)		31	−1.09		−1.17
			388.138	0.092(7)	59(5)		33	−0.88		−1.12
			400.748	0.067(6)	43(4)		32	−0.98		−1.11
			415.521	0.17(1)	107(8)		40	−0.56		−0.99
			477.865	w	w			w		
			490.073	0.06(2)	35(9)		4.9	−0.90		−1.75
			505.773	0.11(1)	73(8)		11	−0.55		−1.36
			595.583	0.04(1)	25(9)			−0.88		
			757.225							
28540.119	5.5	21.5(7)	380.089	0.14(1)	80(7)		59	−0.76		−0.89
			392.239	0.36(2)	201(13)		170	−0.33		−0.40
			405.886	0.100(9)	56(5)		31	−0.86		−1.11
			413.892	0.023(5)	13(3)		3.7	−1.48		−2.02
			430.495	0.092(9)	52(5)		24	−0.84		−1.17
			522.499	0.012(2)	6.5(1.4)			−1.57		
			545.529	0.010(3)	5.6(1.8)			−1.60		
			568.672	0.031(5)	18(3)			−1.07		
			596.883	0.026(6)	15(3)		7.7	−1.10		−1.38
			606.079	w	w			w		
			636.827	0.037(8)	21(5)		4.9	−0.90		−1.52

Table 3. (*concluded*).

Upper level energy (cm^{-1})	J	Lifetime (ns)	Transition wavelength (nm)	Branching ratio	$g_u A_{ul}$ (10^6 s^{-1}) This work	XSQGB[a]	CB[b]	log($g_l f_{lu}$) This work	XSQGB[a]	CB[b]
			663.228	0.08(1)	43(6)			−0.54		
			669.356	0.09(1)	48(7)		17	−0.49		−0.93
28725.529	4.5	38.1(2)	367.052	0.034(3)	8.8(9)			−1.75		
			377.429	0.029(3)	7.7(8)		23	−1.79		−1.32
			389.406	0.14(1)	37(3)		32	−1.07		−1.14
			396.298	0.15(1)	39(3)			−1.04		
			410.739	0.43(2)	113(5)			−0.54		
			427.085	0.22(2)	57(4)		12	−0.81		−1.50
			498.707	w	w			w		
			517.484	w	w			w		
			562.737	w	w			w		
			576.870	w	w			w		
			627.348	w	w			w		
			668.780	w	w			w		
28913.990	4.5	14.9(1)	364.529	0.097(7)	65(5)		31	−0.89		−1.20
			374.762	0.093(7)	62(5)		39	−0.88		−1.09
			386.568	0.014(1)	9.5(10)		6.7	−1.67		−1.83
			393.359	0.068(5)	46(3)			−0.98		
			407.583	0.24(2)	162(10)		64	−0.40		−0.79
			423.674	0.39(2)	262(13)		97	−0.15		−0.58
			494.062	0.019(2)	13(1)			−1.34		
			512.484	0.030(3)	20(2)			−1.09		
			660.453	0.047(7)	32(5)			−0.68		
28997.141	4.5	9.6(5)	363.427	0.52(3)	542(40)		300	0.03		−0.23
			373.597	0.26(2)	269(25)		130	−0.25		−0.56
			385.329	0.03(1)	31(13)			−1.16		
			422.186	0.017(4)	17(4)			−1.33		
			477.168	w	w			w		
			492.039	0.030(9)	32(10)		12	−0.94		−1.38
			510.309	0.11(3)	112(27)		54	−0.36		−0.68
			589.739[c]	0.025(8)			10			−1.27
			596.323[c]				6.1			−1.48
			616.834	0.011(4)	12(4)		2.9	−1.18		−1.78
			763.177							
29387.869	4.5	59(1)	358.337	0.17(2)	29(4)		31	−1.25		−1.23
			368.221	0.06(2)	10(3)			−1.67		
			386.159	0.05(2)	9.2(2.9)			−1.69		
			415.333	0.63(3)	106(6)		49	−0.56		−0.90
			482.756	0.023(5)	3.9(8)			−1.86		
			640.404	0.06(2)	11(2)			−1.18		

[a]Ref. 14.
[b]Ref. 8.
[c]Unresolved lines in this work.

Table 4. Transition probabilities and oscillator strengths derived from branching-ratio and lifetime data. Data from this work are compared with those of ref. 9. Branches that were observed but were too small to fit are indicated by the letter w. The issue of unobserved branches is discussed in the text.

Upper level energy (cm^{-1})	Lifetime (ns)	J	Transition wavelength (nm)	$g_u A_{ul}$ (10^6 s^{-1})		$\log(g_l f_{lu})$	
				This work	SW[a]	This work	SW[a]
27695.961	24.6(5)	6.5	420.291	38(4)	160	−0.998	−0.373
			446.734	513(12)	672	0.187	0.300
			602.174	3.4(0.9)	3.4	−1.732	−1.745
			628.563				
			702.574				
			734.475		18		−0.836
			757.810	14(3)	28	−0.905	−0.629
			902.242				
			970.224				
28072.330	9.96(9)	3.5	367.082	248(14)	120	−0.300	−0.618
			376.071	163(11)	92	−0.462	−0.710
			393.843	w	1.8	w	−2.398
			406.832	86(6)	38	−0.670	−0.189
			422.066	176(11)	29	−0.328	−1.114
			486.539		14		−2.301
			499.203	30(3)	11	−0.952	−1.377
			515.504	83(7)	14	−0.479	−1.244
			581.266				
			599.465	18(5)	4.0	−1.022	−1.658
			623.766		4.0		−1.638
			644.753				
			699.340		51		−0.425
28997.141	9.6(5)	4.5	363.427	542(40)	300	0.031	−0.230
			373.597	269(25)	160	−0.249	−0.475
			385.329	31(13)		−1.162	
			422.186	17(4)	4.2	−1.332	−1.950
			477.168	w	1.8	w	−2.211
			492.039	32(10)		−0.938	
			510.309	112(27)	73	−0.357	−0.545
			589.739		6.1		−1.498
			596.323		6.8		−1.440
			616.834	12(4)	3.6	1.181	−1.687
			763.177		2.9		−1.596

[a] Ref. 9.

References

1. G.M. Wahlgren. Phys. Scr. T, **100**, 22 (2002).
2. E. Biémont and P. Quinet. Phys. Scr. T, **105**, 38 (2003).
3. C.R. Cowley, T. Ryabchikova, F. Kupka, D.J. Bord, G. Mathys, and W.P. Bidelman. Mon. Not. R. Astron. Soc. **317**, 299 (2000).
4. S. Vauclair. Space Sci. Rev. **85**, 161 (1998).
5. J.J. Curry, E.A. Den Hartog, and J.E. Lawler. J. Opt. Soc. Am. B, **14**, 2788 (1997).
6. W.F. Meggers, C.H. Corliss, and B.F. Scribner. NBS Monograph 32, Parts I and II. U.S. Government

Printing Office, Washington, DC. 1961.
7. W.F. Meggers, C.H. Corliss, and B.F. Scribner. NBS Monograph 145, Parts I and II. U.S. Government Printing Office, Washington, DC. 1975.
8. C.H. Corliss and W.R. Bozman. Monograph 53. U.S. National Bureau of Standards, Washington, DC.
9. L. Saffman and W. Whaling. J. Quantum. Spectrosc. Radiat. Trans. **21**, 93 (1979).
10. T. Andersen, O. Poulsen, T.S. Ramanujam, and A.P. Petkov. Sol. Phys. **44**, 257 (1975).
11. R.L. Kurucz and B. Bell. Atomic line data. Kurucz CD-ROM No. 23. Smithsonian Astrophysical Observatory, Cambridge, Mass. 1995.
12. http://cfa-www.harvard.edu/amdata/ampdata/kurucz23/sekur.html
13. A. Kastberg, P. Villemoes, A. Arnesen, F. Heijkenskjöld, A. Langereis, P. Jungner, and S. Linnæus. Z. Phys. D, **28**, 289 (1993).
14. H.L. Xu, S. Svanberg, P. Quinet, H.P. Garnir, and E. Biémont. J. Phys. B: At. Mol. Phys. **36**, 4773 (2003).
15. http://w3.umh.ac.be/~astro/dream.shtml
16. T.J. Scholl, R.A. Holt, D. Masterman, R.C. Rivest, S.D. Rosner, and A. Sharikova. Can. J. Phys. **80**, 1621 (2002).
17. Z. Zhiguo, Z.S. Li, H. Lundberg, K.Y. Zhang, Z.W. Dai, J. Zhankui, and S. Svanberg. J. Phys. B: At. Mol. Opt. Phys. **33**, 521 (2000).
18. W. Demtröder. Laser spectroscopy. Springer, Berlin. 1996.
19. S.L. Kaufman. Opt. Commun. **17**, 309 (1976).
20. J.L. Hall and S.A. Lee. Appl. Phys. Lett. **29**, 367 (1976).
21. L.H. Cadwell. Am. J. Phys. **64**, 917 (1996).
22. P.M. Kock, L.D. Gardner, and J.E. Bayfield. *In* Beam-foil spectroscopy. Vol. 2. *Edited by* I.A. Sellin and D.J. Pegg. Plenum, New York. 1976. p. 829.
23. L. Kay and R. Shepherd. J. Phys. E: Sci. Instrum. **16**, 295 (1983).
24. W.C. Martin and W.L. Wiese. *In* Atomic, molecular, & optical physics handbook. *Edited by* G.W.F. Drake. AIP, New York. 1996.

Appendix A. Fiber array design

In this experiment it is very important that the observed LIF intensities be accurately proportional to the Einstein A coefficients for spontaneous emission. Excitation of ions by a linearly polarized laser beam produces unequal populations in the Zeeman sublevels of the upper state, characterized as an alignment, resulting in an anisotropic radiation pattern. The practical impossibility of constructing an impartial 4π-solid-angle LIF detector introduces a potential bias into branching-ratio measurements. In this Appendix, we show that this source of systematic error can be eliminated by careful design of the detection system, and present two different solutions to the problem, both of which were implemented in our apparatus.

Consider a transition from a given upper level u with angular-momentum quantum numbers J_u, $M_u = J_u, J_u - 1, \ldots, -J_u$ to a given lower level ℓ with corresponding quantum numbers J_ℓ, $M_\ell = J_\ell, J_\ell - 1, \ldots, -J_\ell$. We take the $\hat{z}$-axis along the direction of the electric field of the laser radiation. The upper-level populations $P(M_u)$ created by absorption of laser photons will be unequal, and are assumed to be *completely arbitrary*. The electric-dipole selection rules allow a given sublevel M_u to decay to (at most) three lower levels, $M_\ell = M_u + \Delta M$ where $\Delta M = 0, \pm 1$, with relative probabilities given [A.1]by the squared Clebsch–Gordan coefficients $|\langle J_u, M_u, 1, \Delta M \mid J_\ell, M_\ell \rangle|^2$. These three $\Delta M = 0, \pm 1$ transitions have electric-dipole angular distributions [A.1] given by

$$S_{\Delta M}(\theta) = \begin{cases} \left(\frac{3}{8\pi}\right) \sin^2 \theta, & \Delta M = 0 \\ \left(\frac{3}{8\pi}\right) \frac{1}{2} \left(1 + \cos^2 \theta\right), & \Delta M = \pm 1 \end{cases} \tag{A1}$$

The total rate of spontaneous emission from a particular sublevel M_u via the branch $u \rightarrow \ell$ is given by the product $P(M_u) A_{u\ell}$. To calculate the rate of emission into the solid angle $\sin\theta \, \mathrm{d}\theta \, \mathrm{d}\phi$, we multiply this by the electric-dipole angular-distribution function, which can be obtained by summing the three $\Delta M = 0, \pm 1$ angular distributions weighted by the corresponding squared Clebsch–Gordan coefficients. The radiation pattern is independent of the azimuthal angle φ. Thus

$$I_{M_u}(\theta,\phi) = P(M_u)\,A_{ul} \sum_{\Delta M=0,\pm 1} |\langle J_u, M_u, 1, \Delta M \mid J_l, M_l\rangle|^2\, S_{\Delta M}(\theta) \tag{A2}$$

The total detected intensity I_{total} can then be obtained by integrating the product of this angular distribution with the angular efficiency function of the detector, $\varepsilon(\theta,\phi)$ and summing over M_u

$$I_{\text{total}} = \sum_{M_u=-J_u}^{J_u} \int_0^{2\pi}\int_0^{\pi} \varepsilon(\theta,\phi)\; I_{M_u}(\theta,\phi)\sin\theta\, d\theta\, d\phi \tag{A3}$$

Suppose we had a detector that responded impartially over the full 4π solid angle, i.e., $\varepsilon(\theta,\phi) =$ constant $\equiv \varepsilon_0$. Then, because

$$\int_0^{2\pi} d\phi \int_0^{\pi} S_{\Delta M}(\theta)\sin\theta\, d\theta = 1 \tag{A4}$$

for *any* ΔM

$$\begin{aligned} I_{\text{total}} &= \sum_{M_u=-J_u}^{J_u} \int_0^{2\pi}\int_0^{\pi} \varepsilon_0\; P(M_u)\; A_{ul} \sum_{\Delta M=0,\pm 1} |\langle J_u, M_u, 1, \Delta M \mid J_l, M_l\rangle|^2\, S_{\Delta M}(\theta)\,\sin\theta\, d\theta\, d\phi \\ &= \sum_{M_u=-J_u}^{J_u} P(M_u)\; A_{ul}\, \varepsilon_0 \sum_{\Delta M=0,\pm 1} |\langle J_u, M_u, 1, \Delta M \mid J_l, M_l\rangle|^2 \\ &= \sum_{M_u=-J_u}^{J_u} P(M_u)\, A_{ul}\, \varepsilon_0 \end{aligned} \tag{A5}$$

in which we have used the orthonormality of the Clebsch–Gordan coefficients. Since the total population $\sum_{M_u} P(M_u)$ is the same for all branches from a common upper level we obtain a total intensity proportional to the Einstein A coefficient. The challenge in the present experiment is to obtain the correct intensities without having an impartial 4π-steradian detector.

We have found two experimental designs that overcome this difficulty. The first makes use of a detector placed at the "magic" angle that has been applied in fields as diverse as electron energy-loss spectroscopy (EELS) [A.2], NMR spectroscopy [A.3], and Raman scattering from liquids [A.4]. This is simply the angle $\theta_{\text{magic}} = \cos^{-1}\left(1/\sqrt{3}\right) \approx 54.7°$ at which $\sin^2\theta_{\text{magic}} = 1/2\left(1+\cos^2\theta_{\text{magic}}\right)$. At this angle $S_{\Delta M}\left(\theta_{\text{magic}}\right) = 1/4\pi$ for *any* ΔM and can be removed from the sum; the orthonormality of the Clebsch-Gordan coefficients then yields

$$\begin{aligned} I_{\text{total}} &= \sum_{M_u=-J_u}^{J_u} P(M_u)\, A_{ul}\, \varepsilon\left(\theta_{\text{magic}},\phi\right) \sum_{\Delta M=0,\pm 1} |\langle J_u, M_u, 1, \Delta M \mid J_l, M_l\rangle|^2\, S_{\Delta M}\left(\theta_{\text{magic}}\right) \\ &= \sum_{M_u=-J_u}^{J_u} P(M_u)\, A_{ul}\, \varepsilon\left(\theta_{\text{magic}},\phi\right)\left(\frac{1}{4\pi}\right) \end{aligned} \tag{A6}$$

and is thus proportional to the Einstein A coefficient. In our LIF detector, one set of fibers is arranged at polar angles close to θ_{magic}.

A second solution to the problem is suggested by the solid-angle integration in (A.4). If we were to simply arrange a ring of fibers *uniformly* distributed in θ, we would have an approximate experimental realization of the integral $\int d\theta$; however, if instead we dispose the fibers *non*-uniformly in such a manner as to have a density of fibers $dN/d\theta \propto \sin\theta$, the collected signal from a single ring of fibers will in effect perform the correct 4π solid-angle integration $\int d\theta \sin\theta$ "in hardware".

Numerical studies of both of these techniques verified that neither employment of a finite acceptance angle centred at the magic angle nor the finite approximation to the $\sin\theta$ density distribution had an appreciable effect on obtaining accurate BRs. As a further check, we interchanged the roles of the two sets of fibers in the experiment and found no significant change in the measured BRs, as discussed above.

References

A.1. E.U. Condon and G.H. Shortley. The theory of atomic spectra. Cambridge University Press, London, 1967. Chap. 4, Sect. 5.
A.2. Y. Sun and J. Yuan. Phys. Rev. B, **71**, 125109-1 (2005).
A.3. I.J. Lowe. Phys. Rev. Lett. **2**, 285 (1959).
A.4. L.J. Kaufman, J. Heo, L.D. Ziegler, and G.R. Fleming. Phys. Rev. Lett. **88**, 207402-1 (2002).